



MINISTRY OF TECHNOLOGY
AERONAUTICAL RESEARCH COUNCIL
CURRENT PAPERS

Results and Analysis of Pressure Measurements on
Two Isolated Slender Wings and
Slender Wing-Body Combinations
at Supersonic Speeds
Part 1 - Analysis

By

Mrs. K. A. Fellows and E. C. Carter

A. R. A., Bedford

LONDON. HER MAJESTY'S STATIONERY OFFICE

1970

PRICE 16s 0d [80p] NET

AERONAUTICAL RESEARCH COUNCIL,
NATIONAL PHYSICAL LABORATORY,
TEDDINGTON, MIDDLESEX.

With the Compliments
of the
Publications Officer

November, 1969

Results and Analysis of Pressure Measurements on Two Isolated
Slender Wings and Slender Wing-Body Combinations
at Supersonic Speeds - Part I - Analysis

- By -

Mrs. K. A. Fellows and E. C. Carter,
ARA, Bedford

Summary

As a contribution to the RAE study on guided weapons, this report deals with pressure plotting results on an axisymmetric body and two very slender wings (aspect ratios 0.83 and 0.31) tested in isolation and as wing-body combinations. The tests which were made in the ARA supersonic wind tunnel were at Mach numbers 1.7, 2.0 and 2.8 and incidence angles from 0° to 43°. Full pressure measurements are presented graphically in Part II of this report which may be obtained on request to ARA.

By suitably integrating the pressure coefficients it has been possible to isolate the contributions to the overall normal force made by the wing upper surface, wing lower surface, forebody, cylindrical body and the mutual wing-body interference. Each item has been compared with theoretical and empirical prediction methods currently available. Significant differences between theory and practice were discovered, particularly for the most slender wing, at high pitch angles.

The main features which have been brought to light in this study are as follows. The vortex induced lift on the wing upper surface continues up to very high incidences especially on the most slender wing, with much higher suction than had been predicted. New values of k , the limiting suction level, are proposed and an empirical formula relating the upper surface normal force to Mach number, leading edge sweep angle and pitch angle is suggested for the range of these particular wings. The wing lower surface normal force is well predicted for the less slender configuration by Collingbourne - Ref.2 - but is underestimated for the more slender wing. A modification is proposed to allow for this.

Body interference on the wing falls off rapidly above about 10° to virtually zero at 25° incidence.

There is no loss of non-linear lift on the body due to the presence of the wings.

Contents/

Contents

1. Introduction
 2. Experimental Details
 3. Presentation of Pressure Data
 - 3.1 Integrations
 4. Upper Surface Non-Linear Normal Force
 5. Lower Surface Non-linear Normal Force
 6. Total Normal Force for Wings
 7. Mutual Interference between *wing* and Body
 - 7.1 Comparison with balance measurements
 - 7.2 Theoretical methods
 - 7.3 Empirical methods
 8. Conclusions
- Notation
- References
- Acknowledgement
- Illustrations - Figs. 1 to 26
-

1. Introduction

The study of slender wing body configurations for guided weapons has called for comprehensive theoretical and experimental studies over an extended range of flight conditions and geometric parameters. These slender configurations are required to develop lift at high angles of incidence where non-linear effects such as wing vortex lift are significant. A large amount of force data has been made available from the generalised RAE study on guided weapons, Ref.1, and various empirical working rules have been proposed for the overall forces on wing body combinations.

An empirical theory for the isolated wing normal force has been proposed by Collingbourne (Ref.2) and the original purpose of the work in the present Report was to verify, by pressure plotting, Collingbourne's predictions for the upper surface normal force on these wings in isolation. Aspects of particular interest were the degree of upper surface suction which could be developed at very high incidence, the existence or otherwise of a wing vortex contribution to normal force when the leading edge normal Mach number exceeded unity and the modifications imposed when the wing was attached to an ogive-cylinder body. In order to cover the limiting conditions of Collingbourne's theory, two different wing sweeps were used corresponding to Wing 1 (78.2°) and Wing 8 (85.5°) of the RAE series. Full pressure coverage of the pressure side of the wing was also obtained from inverted tests to provide further checks with Collingbourne's theory for lower surface normal force on wings. Data obtained with and without a body also provided body-on-wing, and wing-on-body interference factors which could be compared with slender body and other theories in Ref.10 (Nielsen). The derivation of interference factors at very high incidence was originally precluded by the lack of available data on ogive cylinder-bodies. Additional tests were made on the nose-body combination to determine normal forces for incidences greater than 25° .




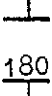





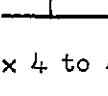
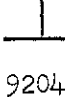

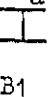



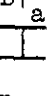

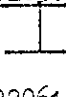

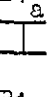

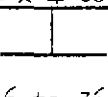
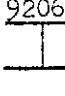

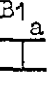
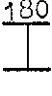
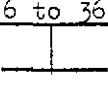



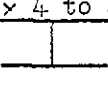



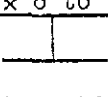
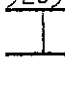


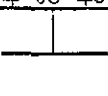
In addition to the derived aerodynamic force data, the detailed pressure distributions in Part II provide the basic data for readers who wish to make their own analysis of the aerodynamics, and load and stressing information for design offices.

As a simplified means of obtaining a qualitative picture of the wing vortices a limited series of photographs were taken using the vapour screen technique.

2. Experimental Details

The wind tunnel tests were completed in December, 1968. Two wings, (Wing 1 and Wing 8 of the RAE series, aspect ratios 0.83 and 0.31 respectively) have been tested both in isolation and mounted on the pressure plotted body B1_a(Fig.1a). Wing 1 has 26 pressure tappings on one surface of one wing and Wing 8 has 30 tappings. Figure 1b shows the tube positions on the wings and body and the following table gives details of the Mach numbers and incidence angles of the tests.

CONFIG.NO./

CONFIG.NO.	WING	BODY	M	ϕ	θ_{NOM}
<u>92011/2/3/4</u> 	<u>8</u> 	-	1.7	<u>0</u>	<u>0 x 6 to 36, 42$\frac{1}{2}$</u>
			2.0		<u>-6,0,6,12,16 x 2 to 40,42$\frac{1}{2}$</u>
			2.8		<u>-6,0,6,12 x 2 to 40,42$\frac{1}{2}$</u>
<u>92021</u> 	<u>8</u> 	-	1.7	<u>180</u>	<u>0 x 6 to 36, 42$\frac{1}{2}$</u>
			2.0		
			2.8		
<u>92031</u> 	<u>1</u> 	<u>B1_a</u> 	2.0	<u>0</u>	<u>-6,0 x 4 to 40,43$\frac{1}{2}$</u>
			2.8		<u>-6,0 x 4 to 40,42$\frac{1}{2}$</u>
<u>92041</u> 	<u>1</u> 	<u>B1_a</u> 	2.0	<u>180</u>	<u>0 x 6 to 36, 43$\frac{1}{2}$</u>
			2.8		<u>0 x 6 to 36, 42$\frac{1}{2}$</u>
<u>92051/2</u> 	<u>8</u> 	<u>B1_a</u> 	2.0	<u>0</u>	<u>-6,-4 x 4 to 40,43$\frac{1}{2}$</u>
			2.8		
<u>92061</u> 	<u>8</u> 	<u>B1_a</u> 	2.0	<u>180</u>	<u>-6 x 6 to 36, 43$\frac{1}{2}$</u>
			2.8		
<u>92071</u> 	<u>1</u> 	-	2.0	<u>0</u>	<u>-6,0 x 4 to 40, 43$\frac{1}{2}$</u>
			2.8		
<u>92081</u> 		-	2.0	<u>180</u>	<u>-4,0 x 6 to 36, 43$\frac{1}{2}$</u>
			2.8		
<u>92091</u> 	-	<u>B1_a</u> 	2.0	<u>0</u>	<u>-4 x 4 to 40, 43$\frac{1}{2}$</u>
			2.8		

The incidence angles quoted are those of the supporting quadrant and are accurate for all tests on the wing/body combinations. However, the sting support for the wing alone cases was more flexible and deflection calibrations indicated a small increase in incidence angle under load for Wing 8. Wing 1, having a larger planform area, deflected considerably more (up to 2° at the highest angles). This could be seen from schlieren photographs and measured angles agreed quite well with calculated deflections. Unlike Wing 8, Wing 1 was tested without a strengthening spine (Fig.1a) and the apex was seen to bend at the highest angles of attack. By this stage, however, the shocks from the tunnel support system were interfering with the flow over the rear of the wing so that the pressure measurements were invalid.

Two quadrants of the body were pressure plotted and so duplicate information was obtained from the model upright and inverted tests on the parallel section. (The forebody pressures were not recorded in the presence of the wings).

The pressures were measured by a stepping scanivalve system having the ability to stop on each tube and allow the pressure to settle before recording the level. The scanivalves were situated outside the tunnel and connections made by flexible tubing. A continuously operating vacuum pump was connected to one port of each scanivalve by a very short length of tubing to act as a check on the accuracy of the scanivalve at vacuum conditions and provide a low level datum. The absolute pressure in this line was measured by a McLeod gauge as 0.1 mm of mercury. The scanivalve measured this as vacuum within an experimental accuracy of ± 0.5 mm Hg (0.02"). This exercise confirmed that the very low pressures of the order of 3 mm Hg (0.12"), measured on the upper surface of the wings, were correct to the above accuracy. Repeat test results were in very close agreement with the original even when asymmetric vortex shedding was apparent.

The Mach number 1.7 was omitted from the later tests after a preliminary investigation had shown that these results did not cover the main region of interest.

Vapour screen photographs showing the flow pattern above two of the configurations at about $2/3$ wing root chord are presented in Figs.1c and d. It was noted visually that the pattern of behaviour of the vortices with incidence varied little with Mach number. Considering Fig.1c, on the wing alone at 10° , two circular vortices had formed curling from the leading edge. With increase of incidence, the shape deepened to oval at 15° and became pear shaped at 17° . By 18° one vortex had stretched more than the other and then the tip detached forming a third vortex above the other two. This left the vortex on the opposite side taller than the first one. In turn its tip detached forming a fourth vortex. This process repeated itself with increase of incidence until by 28° a family of staggered vortices could be seen. At incidences above 15° the existence of strong shock waves on the expanding flow around the vortices is noted. At higher angles the vortices coalesced into a large region of separated flow. For the wing-body combinations, Fig.1d, the vortex pattern remained symmetrical throughout the incidence range.

3. Presentation of Pressure Data

In Part II, spanwise pressure distributions for the wing alone and in the presence of the body are plotted in Figs.2, 3, 4 and 5 for Wing 8 upper surface, Wing 8 lower surface, Wing 1 upper surface and Wing 1 lower surface respectively. Nominal values of α are quoted but the isolated wings were at slightly higher angles due to sting bending. The deflection varied with M , α and planform, a typical value being 2.2° at $\alpha_{\text{Nominal}} = 30^\circ$, $M = 2.8$ for Wing 1, and 0.8° for Wing 8. Corrected pitch angles are used with the integrated results.

The effects of the two wings on the body can be seen in Figs.6a,b. The two sets of results for the body in the presence of Wing 1 were obtained from the upright and inverted tests. For Wing 8, three sets of results were available but these were so similar that only a mean value has been plotted. In Figs.6c and d the three rows of pressures on the forebody are plotted separately since they were measured at a later stage.

Some/

Some information has been omitted at the highest incidences where it was obvious that support interference was taking place.

A typical example of each Figure is included in Part I.

3.1 Integrations

Areas were allocated to each pressure point and $C_p \times$ area integrated numerically. The boundaries of the areas were midway between adjacent tubes where possible. In the absence of a better estimate on the wings, the outermost pressure on each spanwise row was assumed to act up to the leading edge.

A check on the validity of the method of integration has been made by plotting along generators from apex to trailing edge. The profiles were so flat that integration graphically along the generators would not improve the estimates made by area weighting. The main region of doubt, whatever the integration method is the forward outboard area where the wings were too thin to install tubes. If the spanwise profile in this region were assumed to be the same as on the rear part of the wing, the 'wing alone' integrations could be increased slightly and the 'wing in presence of the body' integrations could be reduced. The changes involved would be too small to affect the arguments put forward in the later sections of this note and the assumption of spanwise similarity (conical flow) is not necessarily valid on the chamfered apex.

4. Upper Surface Non-Linear Normal Force

The upper surface pressures from the wing alone tests have been integrated and C_{N_u} for each of Wings 1 and 8 is plotted against incidence (corrected for deflections) in Fig.7. The results are compared with Collingbourne's theory of Ref.2 in this figure and again in parametric form in Fig.8.

Collingbourne splits the upper surface normal force into the linear and non-linear components as follows.

$$C_{N_u} = \frac{a}{2} \alpha + b_u \alpha^2 \quad \text{where } a \text{ is the linear theory lift curve slope.}$$

He further postulates that

$$b_u = (b_u)_h + (b_u)_v$$

where $(b_u)_h \alpha^2$ is defined as the hypersonic component (because it tends to a hypersonic limit) and $(b_u)_h$ equals $\frac{-\gamma(Ma)^2}{32k}$. It can be seen from the data

plotted in Figs.7 and 8 that the value of 0.7 for $k = \left[\frac{(-C_{P_{MAX}})}{(-C_{P_{VAC}})} \right]$

proposed in Ref.2 is greatly exceeded in practice. Minimum values of k at the three test Mach numbers were measured as:-

M	1.7	2.0	2.8
k	0.83	0.86	0.91

It/

It was not possible to discriminate between the values of k measured on these two slender wings so the values given above were used for all the calculations on the ARA results. However when comparing these results with other data in Fig.9, it would seem that wing planform might have considerable influence on the value of k . Collingbourne used a constant value of 0.7 corresponding to the high Mach number range of Relf's³ curve. This curve, shown in Fig.9, was proposed as an upper limit in 1953 as a result of an analysis of very early data on what were presumably low sweep wings. More recent data taken from current non-slender configurations tested at ARA is in close agreement with Relf's curve in the transonic region. However the two points which lie above the curve indicate a higher transonic limiting boundary. In the light of this it would seem reasonable to accept that similar high limits will occur on very slender configurations at supersonic free stream Mach numbers whilst transonic leading edge Mach numbers still exist. The broken line in Fig.9 is therefore recommended for application to slender wings.

The remaining non-linear component of the upper surface normal force is plotted against α in Fig.10. The vortex term was isolated from the experimental data as follows:-

$$(b_u)_v \alpha^2 = C_{N_u} - \frac{a}{2} \alpha - (b_u)_h \alpha^2$$

M	$\sin \epsilon$	1	8
		<u>a</u>	
2.0		1.11	0.465
2.8		1.02	0.446

The linear term 'a' listed in the table was obtained from Fig.3 of Ref.2 and $(b_u)_h$ from the expression above and k experimental. For comparison the 'theoretical' vortex term from Fig.4 of Ref.2 is shown individually and in combination with the hypersonic term calculated using firstly k experimental and secondly $k = 0.7$. In Fig.11 experimental values of $(b_u)_v$ are plotted against

$(\bar{M}_N)_s = \sqrt{(M \cos \Lambda)^2 + (Ma)^2}$ which is a convenient approximation to the Mach number normal to the leading edge for very slender wings. Superimposed is the empirical curve taken from Fig.4 of Ref.2. It appears in the light of this new information that Collingbourne's extrapolation to $(b_u)_v = 0$ at $(\bar{M}_N)_s = 1.2$ is not valid. The value of $(\bar{M}_N)_s$ at which $(b_u)_v$ becomes zero depends on wing planform. For the least slender wing the vortex term has virtually disappeared by $(\bar{M}_N)_s = 1.6$ but for the most slender wing it is still a significant term at the end point of the test range.

Mangler/

Mangler and Smith (Ref.4) give $(b_u)_v \approx 4$ when $\alpha \tan \Lambda = 0$ which infers $\alpha = 0$ for these wings. Assuming this limit holds for compressible flows in which $(\bar{M}_N)_s$ is subsonic, the end points for each set of data in Fig.11 have been fitted at $(\bar{M}_N)_s = M \cos \Lambda$. Whilst this procedure tidies up the ends of the curves in Fig.11 it does not lend itself to formulating an empirical law. It must be remembered that the accuracy of the experimental data is worst at low α and $(b_u)_v$ plays a very small part in the overall normal force on the wing. It is proposed, therefore, that Collingbourne's curve be retained for estimating the vortex term when $(\bar{M}_N)_s < 2/3$.

It is for higher values of $(\bar{M}_N)_s$ that $(b_u)_v$ becomes of more significant interest and in this region an empirical law has been fitted to the experimental data for the range of wing sweep and Mach number at present under discussion.

$$\log_{10} (b_u)_v = 2.4 M \cot \Lambda [1 - 1.5 (\bar{M}_N)_s]$$

It can be seen in Fig.12 that although the straight line fits from this equation do not tend to the proper limits, they agree more closely with the experimental data than did Collingbourne's theory. The empirical expression should give reasonable accuracy for predictions of the vortex term for values of $(\bar{M}_N)_s$ in excess of $2/3$ and $(b_u)_v$ less than unity.

5. Lower Surface Non-Linear Normal Force

For wings with shock detached, Collingbourne postulates that

$$C_{N_\ell} = \frac{a}{2} \sin \alpha \cos \alpha + b_\ell \sin^2 \alpha$$

where b_ℓ is the lower surface normal force coefficient at 90° incidence in a

stream of Mach number $\bar{M}_N = \sqrt{M^2 \cos^2 \Lambda + M^2 \sin^2 \alpha \sin^2 \Lambda}$. Maccoll and Codd,

Ref.5, obtained the expression

$$b_\ell = 0.9054 C_{p_s} - \frac{0.1892}{\gamma \bar{M}_N^2} \text{ for a circular plate}$$

where C_{p_s} is the pitot pressure coefficient corresponding to \bar{M}_N , Fig.14.

In Fig.13, the experimental integrated pressures are compared with C_{N_ℓ} calculated from the above expressions and experimentally derived values of b_ℓ have been plotted in Fig.14. The Wing 1 results agree very closely with the recommended theory for $\bar{M}_N > 1$ but for subsonic normal Mach numbers the experimental values of b_ℓ do not confirm the tendency to level off as did the experimental results of Ref.6. The very slender wing (Wing 8) results lie on a higher curve of the same form as the theoretical line. It is, in fact, much closer to the C_{p_s} curve, probably indicating a planform influence on the original expression for b_ℓ .

6. Total Normal Force for Wings

Ortell (Ref.7) proposes the equation

$$C_N = \alpha + c_{d_c} \sin^2 \alpha$$

for the normal force on a low aspect ratio wing where c_{d_c} , the circular cylinder drag coefficient is the same for all wings. This is plotted against $M \sin \alpha$ in Fig.15. He compared this prediction with a considerable amount of experimental data for delta wings and evolved a correction factor

$$\left(\frac{C_{N_{\text{test}}}}{C_{N_{\text{pred}}}} \right) \text{ to be applied to values calculated by the above formula.}$$

The correlating parameters used by Ortell are $\beta \tan \epsilon$ the usual supersonic linear theory similarity parameter and $\beta \tan \alpha$ which accounts for the effect of leading-edge shock detachment which occurs at fairly low angles of attack for highly swept wings. This correction factor is plotted against $(\beta \tan \epsilon) (\beta \tan \alpha)$ in Fig.16 and the open symbols show the result of dividing the normal force data from this test series by Ortell's predicted values. The closed symbols will be discussed in the next section.

Two methods have now been considered for predicting the total wing normal force. Ortell's prediction together with his correction factor, and Collingbourne's method discussed earlier. These two methods are compared with the experimental data in Fig.17. On the whole, Ortell's prediction is closer to the experimental results except at the highest Mach number and incidence on the most slender wing.

7. Mutual Interference between Wing and Body

7.1 Comparison with balance measurements

From the pressures recorded on the wing/body combinations the wing normal force has been integrated. The body pressures have been integrated to provide normal forces appropriate to the particular comparisons being made. For comparison with the experimental force data integration stopped at the plane of the wing trailing edge. For comparison with theories the carry-over fields of influence appropriate to the particular theory have been used, as indicated in Fig.18. To compare the total result with balance measurements on a similar model with a truncated body (Ref.8) it was necessary to estimate the normal force on the nose. This was taken from Ref.9 which agreed very closely with integrated pressures on the forebody of the body alone. The comparisons shown in Fig.19 for the complete model between the solid and chain dotted lines show closer agreement for Wing 8 than Wing 1 over the limited incidence range of the force tests. In this figure the body cross-sectional area has been used as reference. In all subsequent figures and discussion on wing/body interference the relevant wing area is used.

7.2 Theoretical Methods

Until now most of the experimental data on slender wing/body combinations have been overall forces and moments at incidence angles below 25°. It may have been fortuitous that the overall theoretical estimates

have/

have agreed tolerably well with experimental data in this range. At larger incidence angles agreement would not have been so good. It has already been shown that the wing alone estimates are not very accurate and it will be demonstrated that when separated out, the theoretical values for the interference of the body on the wing do not agree with experimental data especially at high angles of attack.

Integrated pressure results for the wings tested with and without the body are compared in Fig.20. There appears to be some interference from the body at low incidence (more so at $M = 2.0$ than $M = 2.8$) but above 20° this has virtually disappeared in all cases. The low incidence slender body theory and upwash theory interference factors for the body on these wings taken from Ref.10 are given in the following table where

$$C_{N_{W(B)}} = K_{W(B)} C_{N_W}$$

Wing	Slender body theory $K_{W(B)}$	Upwash theory $K_{W(B)}$
1	1.1617	1.300
8	1.3493	1.522

$C_{N_{W(B)}}$ calculated from each of these two theories, using experimental results for C_{N_W} is also plotted in Fig.20. Below 10° of incidence, agreement

between slender body $K_{W(B)} C_{N_W}$ and $C_{N_{W(B)}} (exp't)$ is tolerably good, but at

higher angles the discrepancy is so great that it is obvious that other factors need to be considered. The interference of a forebody on the wings is discussed elsewhere, but it is relevant to note that although only results up to 23° of incidence are given it is clear that this term is negative and rapidly increasing in magnitude with incidence. At $M = 2.0$, $\alpha = 23^\circ$, this quantity is equivalent to a ΔC_N of -0.03 for Wing 1 and -0.08 for Wing 8.

At present, there is no theoretical expression to account for the rest of the discrepancy between the slender body theory curves and the experimental curves in Fig.20 at high incidence values. It is stated in Ref.10 that the upwash theory is not recommended. By dividing the experimental values of $C_{N_{W(B)}}$ by C_{N_W} , an experimental interference factor $K'_{W(B)}$ has been found

for each data point. This is plotted against incidence at the bottom of Fig.21. Also in this figure the contributions to $K'_{W(B)}$ from the two

surfaces of the wing are separated and it can be seen that where interference due to the body exists it is picked up on the upper surface of the wing. It should be remembered that the accuracy is least at the lowest incidence values.

The theoretical interference term on the body due to the wings is confirmed by the experimental results. The normal force on that part of the body shaded in Fig.18 is made up of a term due to the body itself and a body interference term due to the wing.

There/

There are various ideas concerning the loss of lift on the body when the wings are present. Collingbourne in another reference suggests that the non-linear component of the normal force on the body between the wings is cancelled. Roe and Osborne when dealing with not so slender

wings subtract $\left(\frac{S_{B(W)}}{S_{B(W)} + S_N} \right) \times$ body non-linear normal force. Where $S_{B(W)}$ is the planform area of the body between the wings and S_N is the planform area of the nose section. However, following the practice of Ogle⁸ in deriving a theoretical estimate to compare with the experimental data in this note, the full linear and non-linear terms are included.

A 'quasi theoretical' value of the normal force on the part of the body in question, in this case the shaded area of Fig.18, is the sum of two terms. The first term is the normal force measured in the body alone tests and the second term, due to wing interference, is $K_{B(w)} C_{N_w}$. A comparison

between this estimate and the experimental results for the body in the presence of each of the wings is given in Fig.22 and shows good agreement in most cases. Values of $K_{B(w)}$ for slender body theory and values quoted in Ref.10 are listed below. By subtracting the 'body alone' normal force from the experimental 'body in the presence of wings' normal force and dividing by C_{N_w} a mean experimental value for $K'_{B(w)}$ has been obtained and this is included in the table.

$K_{B(W)}$	Slender body theory	Ref.10	$K'_{B(w)}$ Experimental
Wing 1 M = 2.0	0.2783	0.246	0.303
M = 2.8	"	0.232	0.260
Wing 8 M = 2.0	0.6107	0.581	0.779
M = 2.8	"	0.565	0.596

7.3 Empirical methods

Several different empirical methods for the estimation of the normal force on wing-body combinations have been collated elsewhere. Some of these methods infer loss of body non-linear lift and for reasons given above are not discussed here. However, one method which will be referred to as the 'Empirical Method' seems to fit the current results well. It assumes that there is no cancellation of body non-linear lift, and $K_{B(W)}$ retains the theoretical value given in Ref.10 but $K_{W(B)}$ varies with $M \sin \alpha$. When the cross flow Mach number exceeds 0.4, $K_{W(B)}$ is changed by compressibility effects to $K'_{W(B)}$. The empirical expression $\frac{K'_{W(B)} - 1}{K_{W(B)} - 1}$ is plotted against

M/

$M \sin \alpha$ in Fig.23, where $K'_{W(B)}$ is the experimental value discussed in 7.2 and $K_{W(B)}$ is the low incidence value from slender body theory.

Information from similar models to those tested here has been collected and the solid line is the empirical fit to this data. The current information fits remarkably well with less scatter than the data used in deriving the empirical curve. This method assumes that the body cross flow Mach number approaches unity when $M \sin \alpha = 0.4$. The surface Mach number distribution is then assumed to be frozen until $M \sin \alpha$ reaches unity. Figure 24 shows the similarity of this empirical method to the current results, which is especially close for wing 1.

Ortell (Ref.7) predicts the normal force of wing/body combinations from a theoretical equation rather than basing it on experimental wing alone values. His expression is:-

$$C_{N_T} = (K_{W(B)} + K_{B(W)}) a \cdot \alpha + 2\alpha \frac{S_B}{S_W} + c_{d_c} \frac{S_{PLAN}}{S_W} \sin^2 \alpha$$

where $K_{W(B)}$ and $K_{B(W)}$ are the slender body interference factors, S_B is the body cross-sectional area and S_{PLAN} is the planform area of the wing/body combination. c_{d_c} is obtained from Fig.15 as in the wing alone calculations.

The correction factor $\left(\frac{C_{N_{test}}}{C_{N_{pred}}} \right)$ taken from Fig.16 is applied

to C_{N_T} and the overall result is shown in Fig.25. For wing 1 the agreement with experimental results is excellent throughout the incidence range. For Wing 8 there is a 16% discrepancy at $\alpha = 40^\circ$. The current results for the wing/body combinations ratioed to Ortell's prediction are plotted against $(\beta \tan \epsilon) (\beta \tan \alpha)$ as solid symbols in Fig.16. These points are closer to the empirical curve than were the wing alone results discussed earlier.

Returning to Fig.25, the $C_{N_{W(B)}}$ curves are those of Figs.20 and 24 repeated.

The $C_{N_{B(W)}}$ curves from Fig.22 have been included for Wing 1

(Fig.25b) but omitted from Fig.25a (wing 8) for clarity. $C_{N_{W(B)}} + C_{N_{B(W)}}$

is a simple addition of these two curves for the various methods. It is, in fact, the normal force on the wing and that part of the body influenced by the wing. This should not be confused with the normal force on a complete model with forebody having the trailing edge of the body in line with the wing trailing edge - this was dealt with in Fig.19.

It appears from Fig.25 that slender body and upwash theory predictions exceed the experimental values by an amount which increases rapidly with incidence. Ortell's prediction is close to the experimental result for Wing 1 but for Wing 8, the prediction is as far below the experimental result as the slender theory is above it. The most consistently reliable prediction is given by 'the Empirical Method' referred to at the beginning of this section, 7.3.

A single data point ($M = 2.8$, $\alpha = 20^\circ$) has been chosen for the Wing 8 on the body configuration to illustrate the way in which a theoretical estimate may have been made for comparison with balance measurements before the current pressure plotting results were available. Although the total agrees with the balance measurement to within 3%, comparison with the integrated pressure results for the individual component parts shows large discrepancies. Figure 26 helps to summarise the findings of this report and three points should be noted in connection with this figure. The wing-on body interference term is larger for the integrated pressures than for the theoretical estimate simply because the wing normal force is larger. The term marked "parallel body" on the right-hand side of Fig. 26 has been reduced by varying amounts by different authors to suit the theories concerning cancellation of body non-linear lift caused by the presence of the wing. A reduction of this term by 12% would conveniently make the overall prediction agree with the balance measurement in this particular example. If the value for body on wing interference obtained from 'the Empirical Method' is substituted for the slender body value, the overall estimate is reduced by 7% and makes the total C_N 4% smaller than the balance measurement.

8. Conclusions

By integrating pressure measurements made on a body and two slender wings tested separately and in combination it has been possible to isolate the contributions to the overall normal force made by each panel surface and by mutual interference. Each term has been compared with some theoretical and empirical prediction methods currently available.

The wing upper surface normal force is considerably larger than Collingbourne's² estimate especially at large incidence angles on extremely slender wings. This is due to the higher lifting suction under the vortex which is found to continue beyond the point at which the Mach number normal to the leading edge reaches unity - confirmed visually by vapour screen photographs. An empirical formula relating the vortex term to wing sweep angle, free stream Mach number and incidence angle is derived for wings in this range of slenderness.

Values of k (the ratio of measured surface static pressure coefficient to that at vacuum conditions) as large as 0.91 were measured. In all cases the experimental values of k exceeded the value of 0.7 used by Collingbourne.

The lower surface normal force is as predicted by Collingbourne for the less slender wing. However, it would appear that the method underestimates the force on very slender wings, and it is suggested that for these wings a value of the lower surface non-linear term b_ℓ equal to the pitot pressure recovery coefficient at the normal Mach number, be used.

The slender body prediction for wing interference due to the body as recommended by Nielsen¹⁰ is only good for incidence angles below 10° . Above this angle the interference rapidly decreases becoming virtually zero by 25° . 'The Empirical Method' discussed in Section 7.3 fits the data best. It is also interesting to note that any favourable body-on-wing interference that exists is picked up on the wing upper surface rather than the lower surface.

Integrated/

Integrated forebody pressures agreed well with the data sheets prediction. However the normal force on the parallel portion of the body measured in the absence of the wings was slightly less than the estimate but when added to the wing-on-body interference term (using $K_{W(B)}$ from Ref.10) equalled the force measured on the parallel portion of the body when the wing was present. This confirms the view put forward in Ref.8 that there is effectively no cancellation of body non-linear lift due to the wings. Figure 22 of this note illustrates this fact directly. The wing-on-body interference factor recommended by Nielsen gives reasonable results throughout the test range.

An alternative empirical prediction method due to Ortell is also discussed. This includes a term for circular cylinder cross flow drag coefficient as the non-linear contribution and a somewhat arbitrary correction factor to the overall result based on a large amount of experimental data. Crude though it may be, this method predicts wing-alone forces and wing-body combination forces for the least slender wing more accurately than any other method studied. Agreement is not so good for the most slender wing.

Notation/

Notation

a	coefficient of linear term in wing normal force	$\left(\frac{dC_N}{d\alpha} \right)_{\alpha \rightarrow 0}$
A	aspect ratio	
b	coefficient of non-linear term in wing normal force	
Bl _a	body defined in Ref.7 and Fig.1a	
c _{d c}	circular cylinder cross flow drag coefficient	
C _N	normal force coefficient	
C _{N_{B(W)}}	" " " of body in presence of wing	
C _{N_W}	" " " of wing	
C _{N_{W(B)}}	" " " of wing in presence of body	
C _p	pressure coefficient	
C _{p_s}	pitot pressure coefficient	
Hg	mercury pressure reference	
k	ratio of maximum negative static pressure coefficient at vacuum conditions	$-C_{P_{VAC}}$ to that $-C_{P_{MAX}}$
K _{B(W)}	interference factor for wing on body - theoretical	} (additional normal force on body due to presence of wing) / (normal force on isolated wing)
K' _{B(W)}	" " " " " " - experimental	
K _{W(B)}	" " " body on wing - theoretical	} (normal force on wing in presence of body) / (normal force on isolated wing)
K' _{W(B)}	" " " " " " - experimental	
M	Mach number	
\bar{M}_N	Mach number normal to leading edge	$= \sqrt{M^2 \cos^2 \Lambda + M^2 \sin^2 \alpha \sin^2 \Lambda}$
$(\bar{M}_N)_s$		$= \sqrt{(M \cos \Lambda)^2 + (M\alpha)^2}$
S _B	Body cross-sectional area	

S_{B(W)}/

$S_{B(w)}$	Planform area of body between wings
S_N	" " " " nose section
S_{PLAN}	" " " wing/body combination
S_W	Net wing reference area
α	angle of incidence
β	$\sqrt{M^2 - 1}$
γ	ratio of specific heats = 1.4 for air
Λ	leading edge sweep angle
ϵ	wing semi apex angle = $\pi/2 - \Lambda$
θ	pitch angle of sting root
ϕ	roll angle

Suffices

h	hypersonic
l	lower surface
T	total
u	upper surface
v	vortex

Figures/

References

<u>No.</u>	<u>Author(s)</u>	<u>Title, etc.</u>
1	K. G. Winter, E. F. Lawlor and D. R. Andrews	Programme of Tests in the 8ft x 8ft Wind Tunnel and High Supersonic Speed Tunnel on a series of Models relevant to the design of Slender Guided Weapons. RAE Tech Memo Aero.720. A.R.C.23 058. June, 1961.
2	J. R. Collingbourne	An Empirical Prediction Method for Non-Linear Normal Force on Thin Wings at Supersonic Speeds. A.R.C. C.P.662. January 1962.
3	E. F. Relf	Note on the Maximum Attainable Suction on a Body in an Airstream. A.R.C. 16 062. July, 1953.
4	K. W. Mangler and J. H. B. Smith	Calculation of the Flow Past Slender Delta Wings with Leading Edge Separation. RAE Report Aero 2593. A.R.C.19 634 May, 1957.
5	J. W. Maccoll and J. Codd	Theoretical Investigations of the Flow Around Various Bodies in the Sonic Region of Velocities. A.R.C.9315 September 1945.
6	S. F. Hoerner	Fluid-dynamic Drag. Published by the author 1958.
7	A. R. Ortell	Supersonic and Hypersonic Lift of Highly Swept Wings and Wing-body Combinations. Journal of Aircraft. Vol.4, No.1, page 78. January - February, 1967.
8	J. B. Ogle	Force Tests on Four Slender Delta Wing-bodies at Mach numbers from 0.6 to 2.8 and a Method of Predicting the Longitudinal Characteristics. RAE Tech Report No. 66307. A.R.C.28 706. October, 1966.
9	-	Royal Aeronautical Society Data Sheets. Bodies S.010302: S.010304.

<u>No.</u>	<u>Author(s)</u>	<u>Title, etc.</u>
10	William C. Pitts, J. N. Nielsen and G. E. Kaattari	Lift and Centre of Pressure of Wing-body-tail Combinations at Subsonic, Transonic and Supersonic Speeds. NACA Report 1307. 1957.

Acknowledgement

The authors would like to express their appreciation of the encouragement and technical advice given by Mr. J. Ogle of the RAE Aerodynamics Dept.

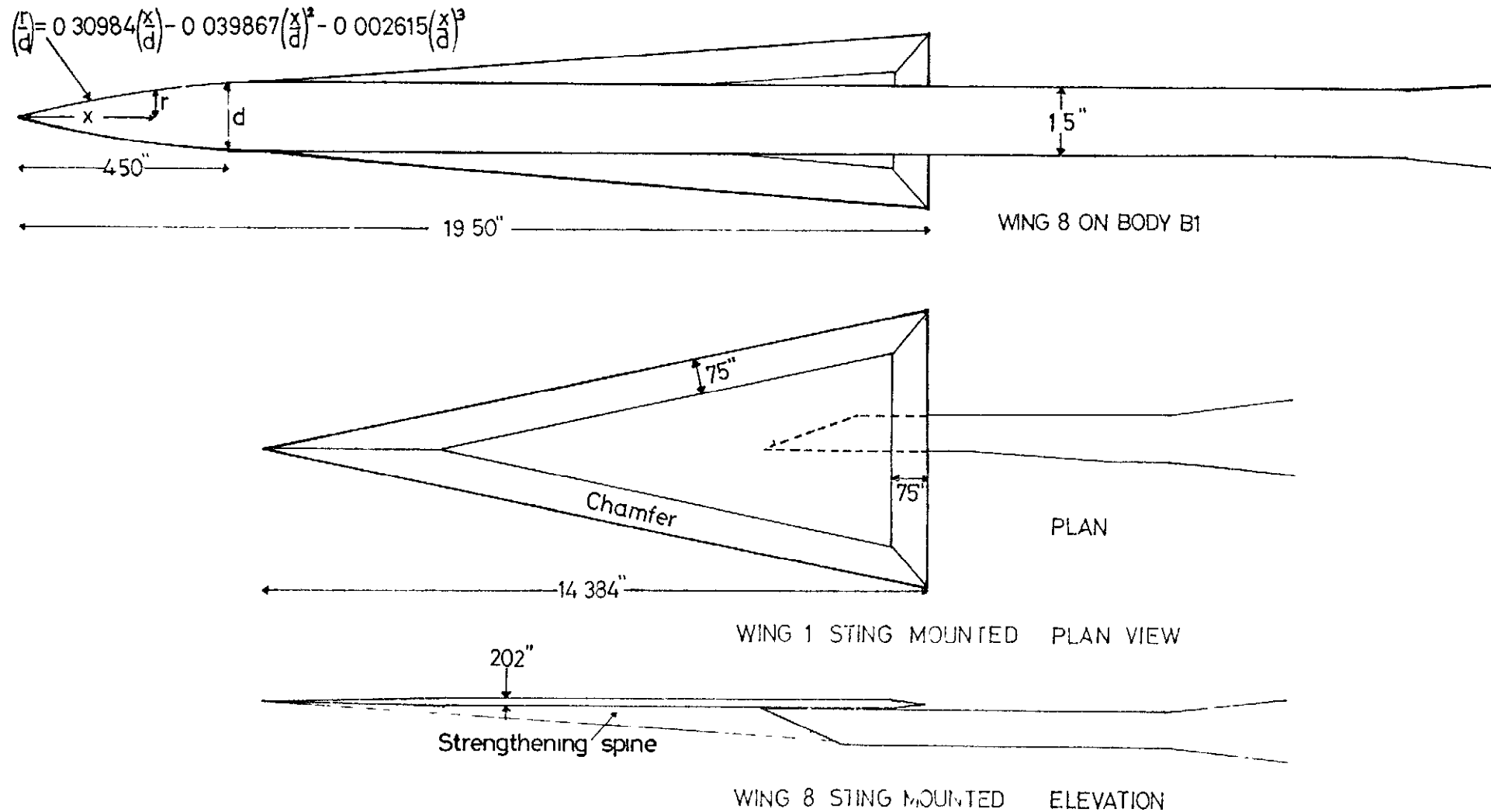


FIG 1a GENERAL ARRANGEMENT OF MODELS 1/3 SCALE

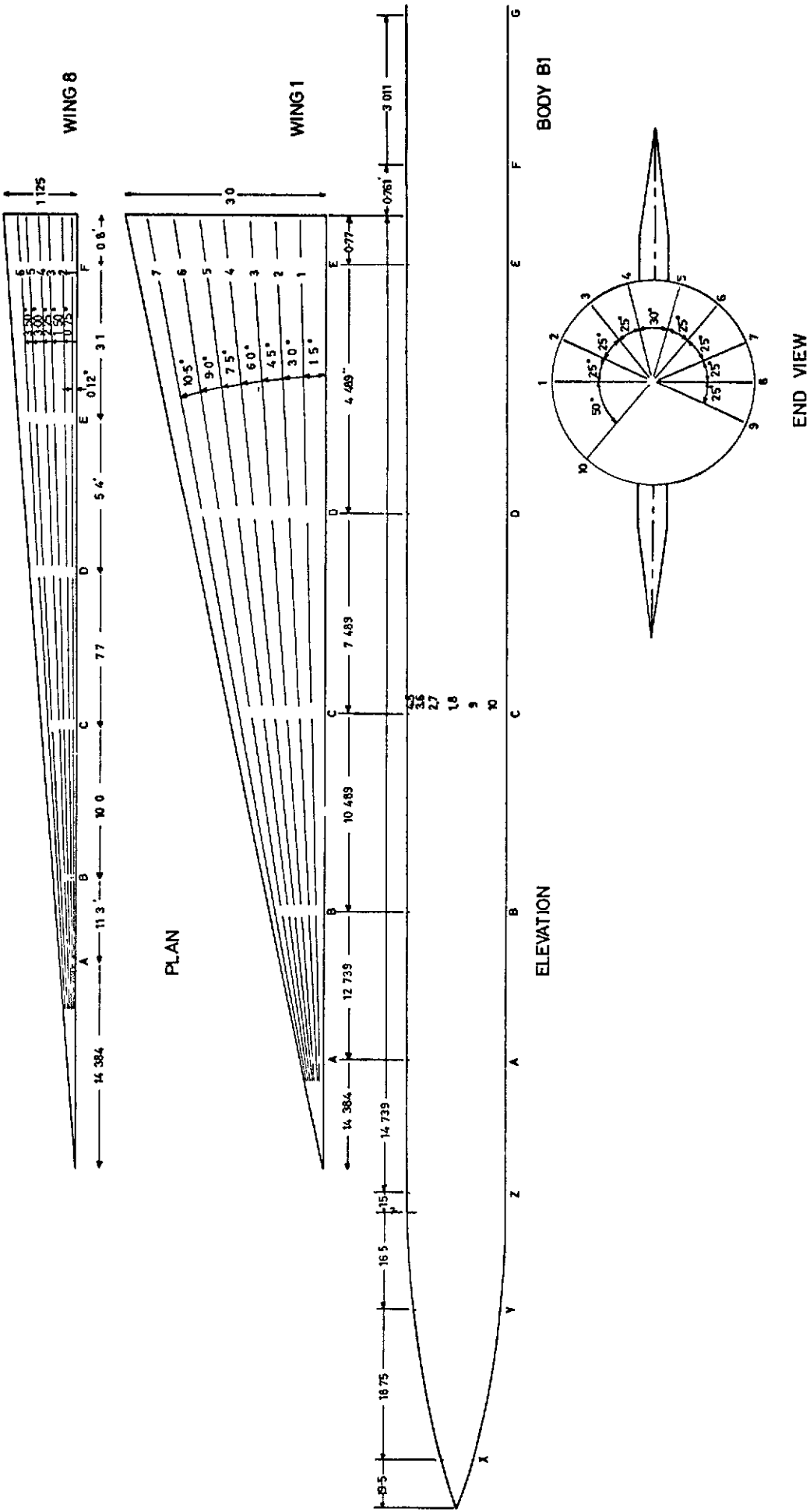


FIG 1b SKETCH SHOWING PRESSURE TUBE LOCATIONS

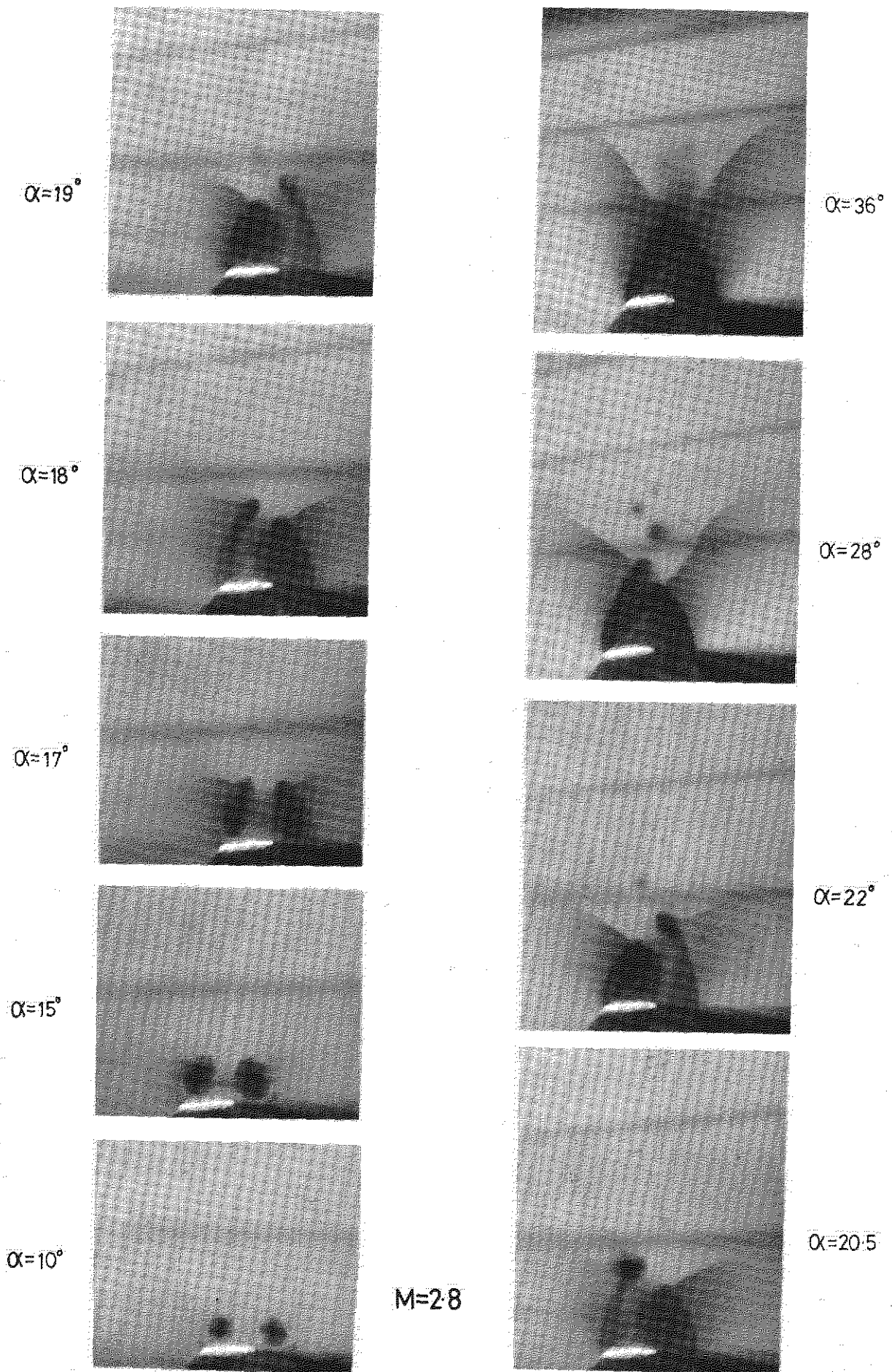


FIG.1c VAPOUR SCREEN PHOTOGRAPHS OF VORTICES ABOVE WING.8

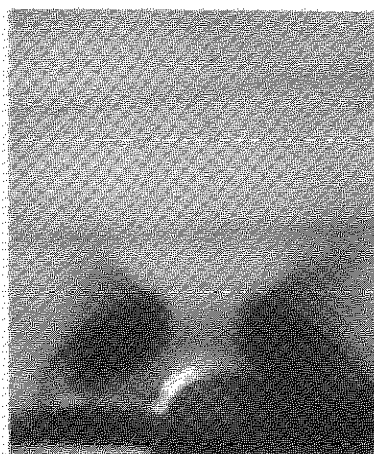
$\alpha=25^\circ$



$\alpha=36^\circ$



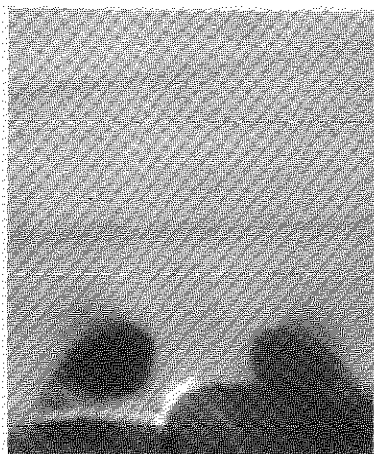
$\alpha=22^\circ$



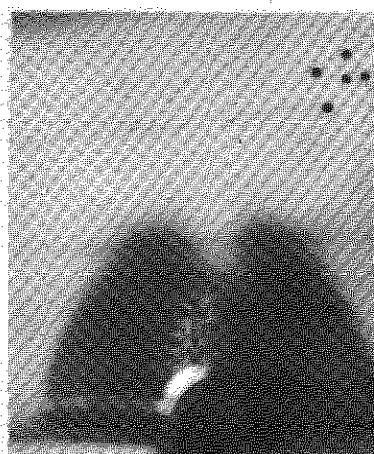
$\alpha=34^\circ$



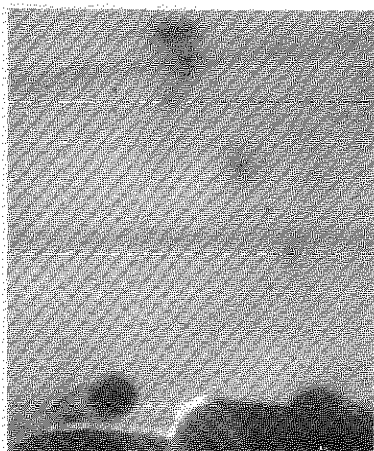
$\alpha=17^\circ$



$\alpha=32^\circ$



$\alpha=10^\circ$



$\alpha=31^\circ$



M=2.0

FIG.1d. VAPOUR SCREEN PHOTOGRAPHS OF VORTICES ABOVE WING 1 AND BODY.

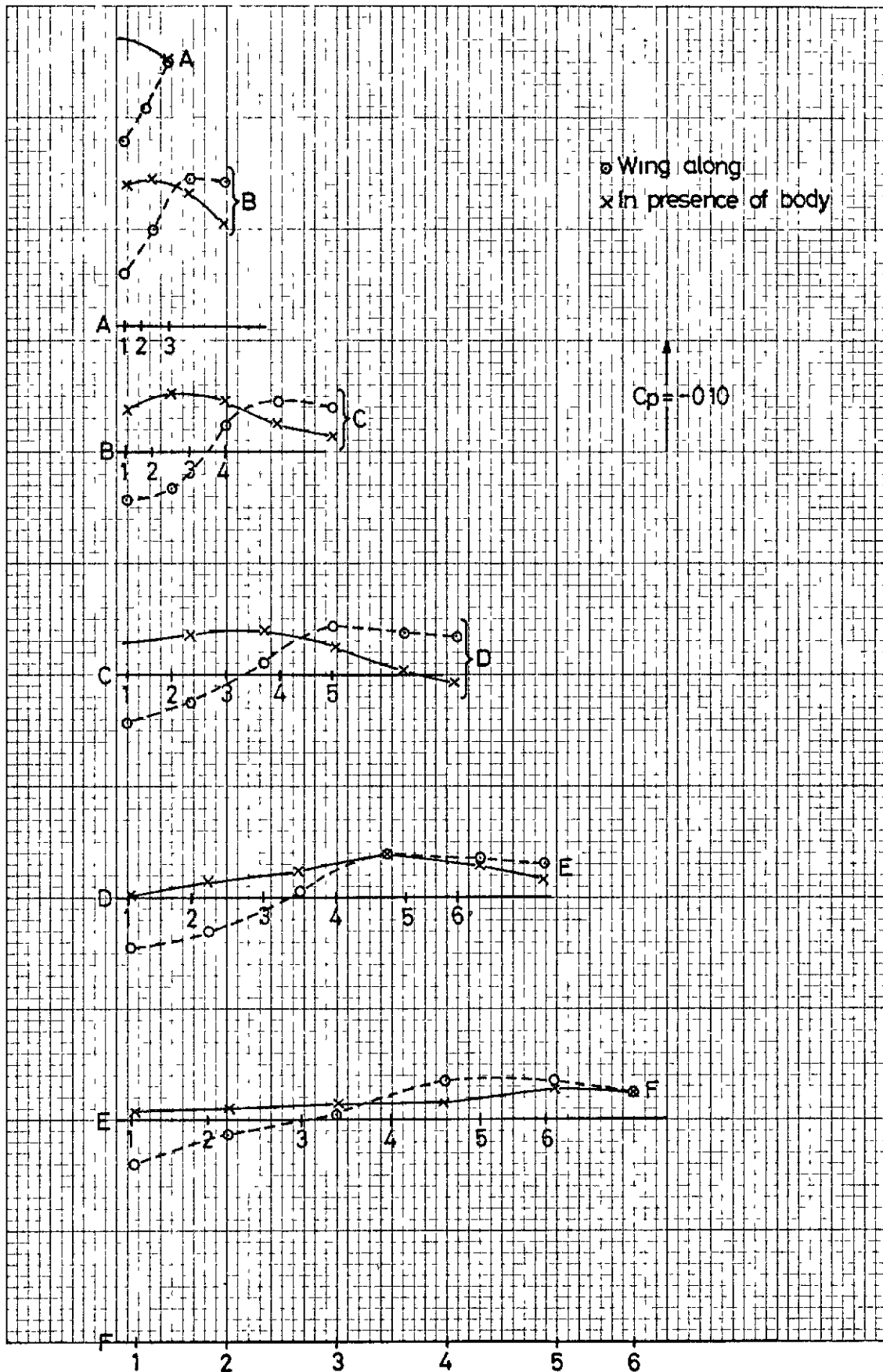


FIG. 2b(vii) WING 8 UPPER SURFACE PRESSURE DISTRIBUTION $M=20$ $\alpha=20^\circ$

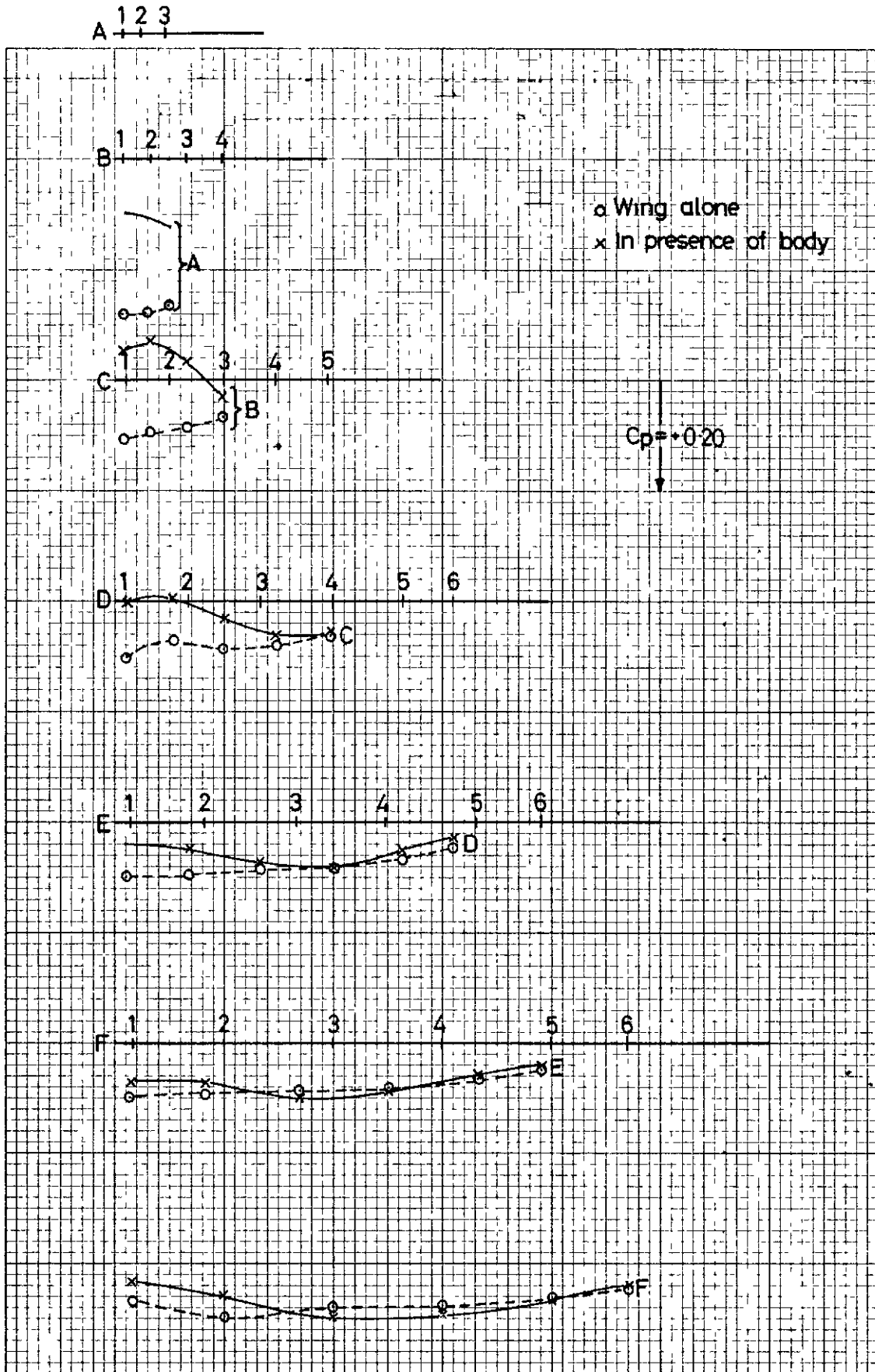


FIG. 3c(vi) WING 8 LOWER SURFACE PRESSURE DISTRIBUTION $M=2.8$ $\alpha=30^\circ$

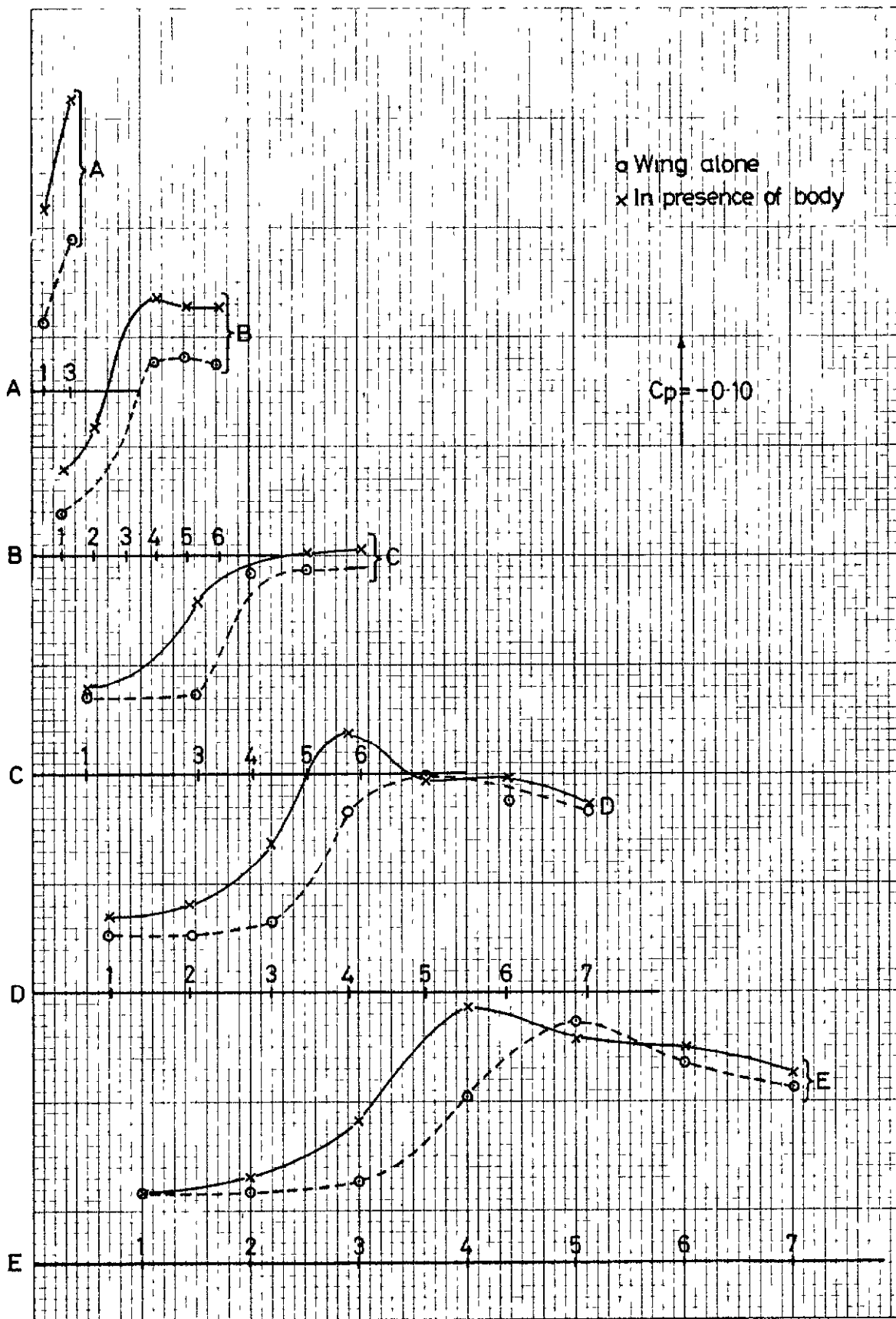


FIG 4a(iii) WING 1 UPPER SURFACE PRESSURE DISTRIBUTION $M=2.0$ $\alpha=8^\circ$

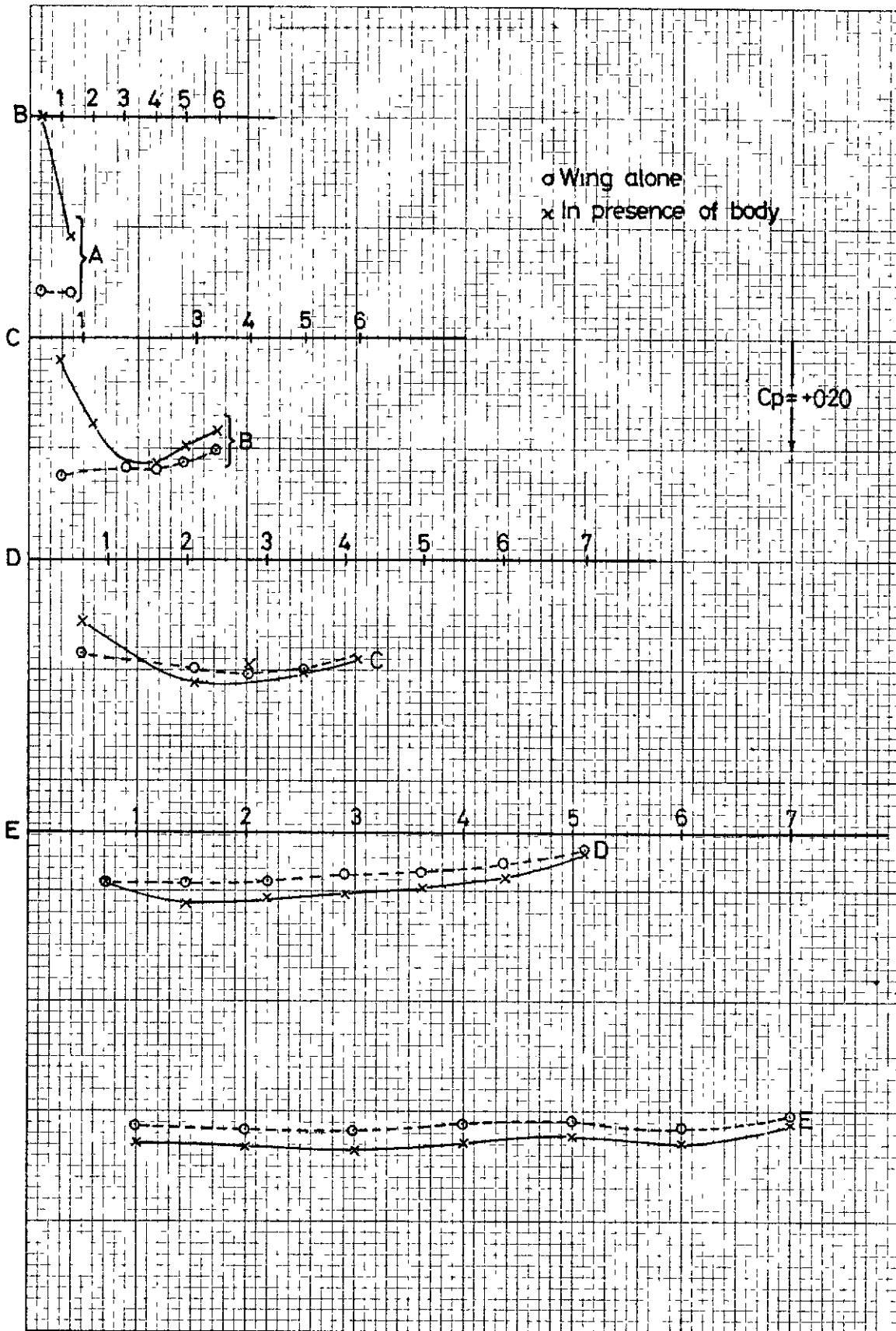


FIG. 5b(vi) WING 1 LOWER SURFACE PRESSURE DISTRIBUTION $M=28$ $\alpha=30^\circ$

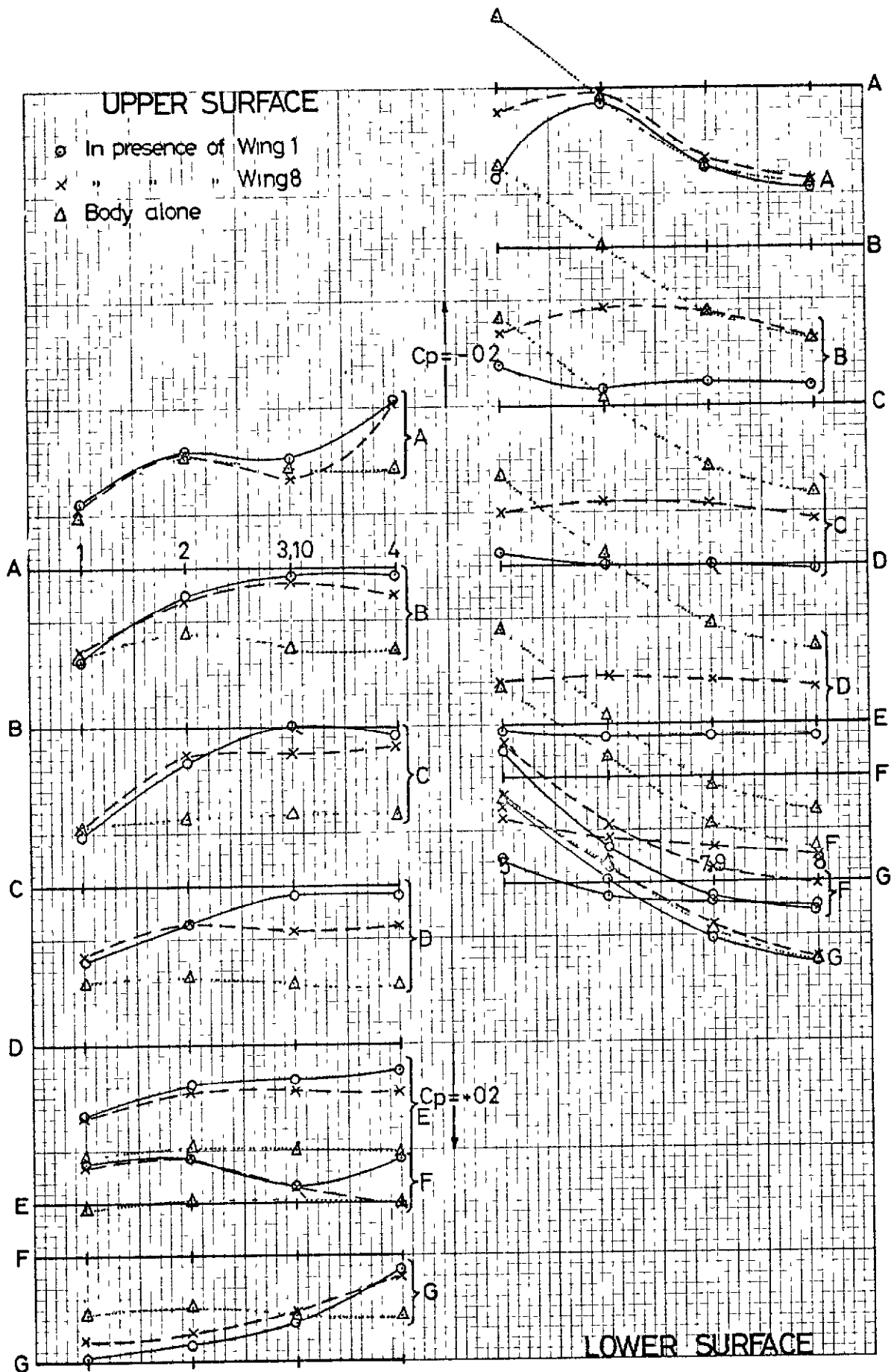


FIG. 6a(viii) BODY PRESSURE DISTRIBUTION. $M=2.0$ $\alpha = 20^\circ$

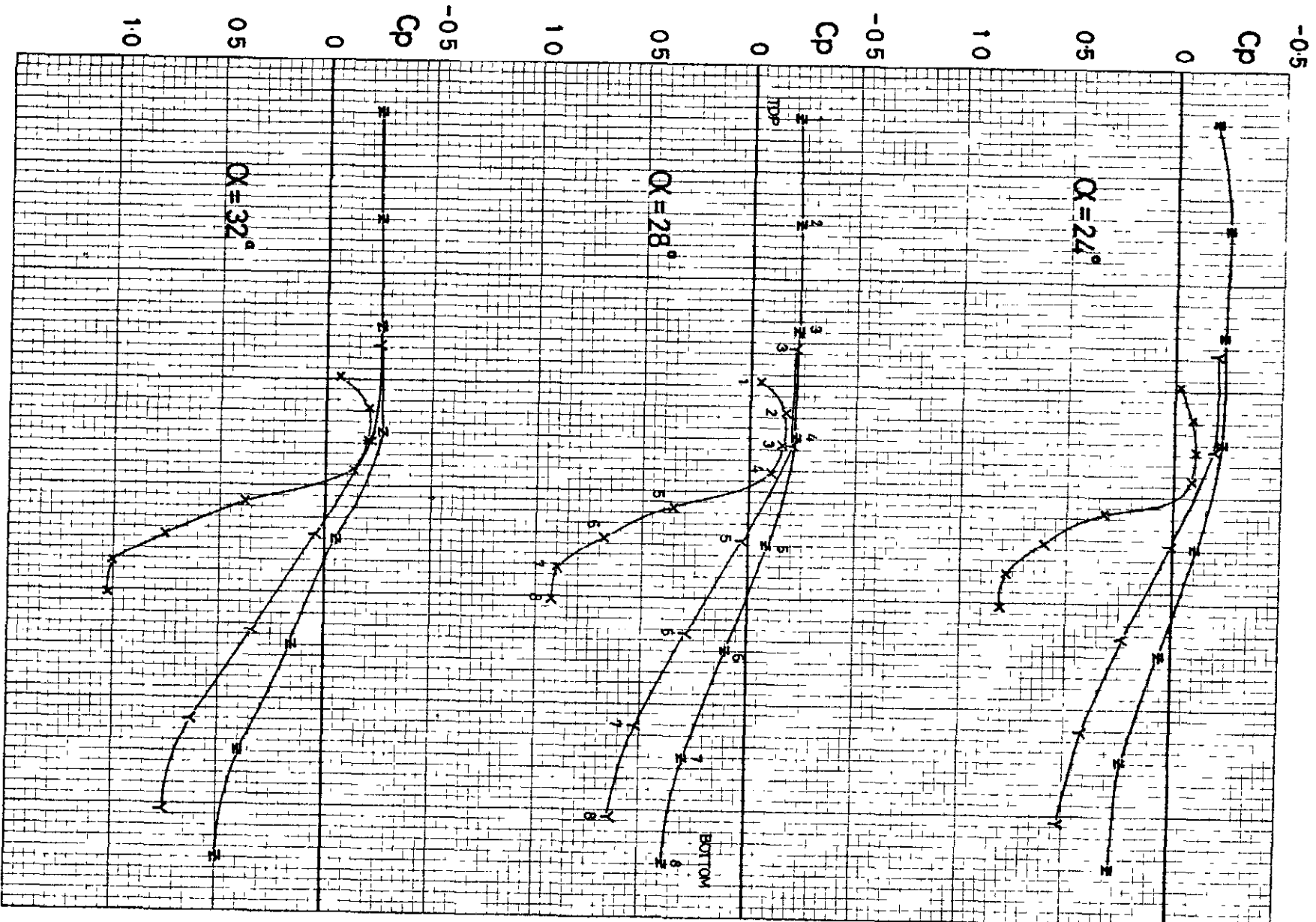


FIG. 6c(iii) FOREBODY PRESSURE DISTRIBUTION $M = 2.0$

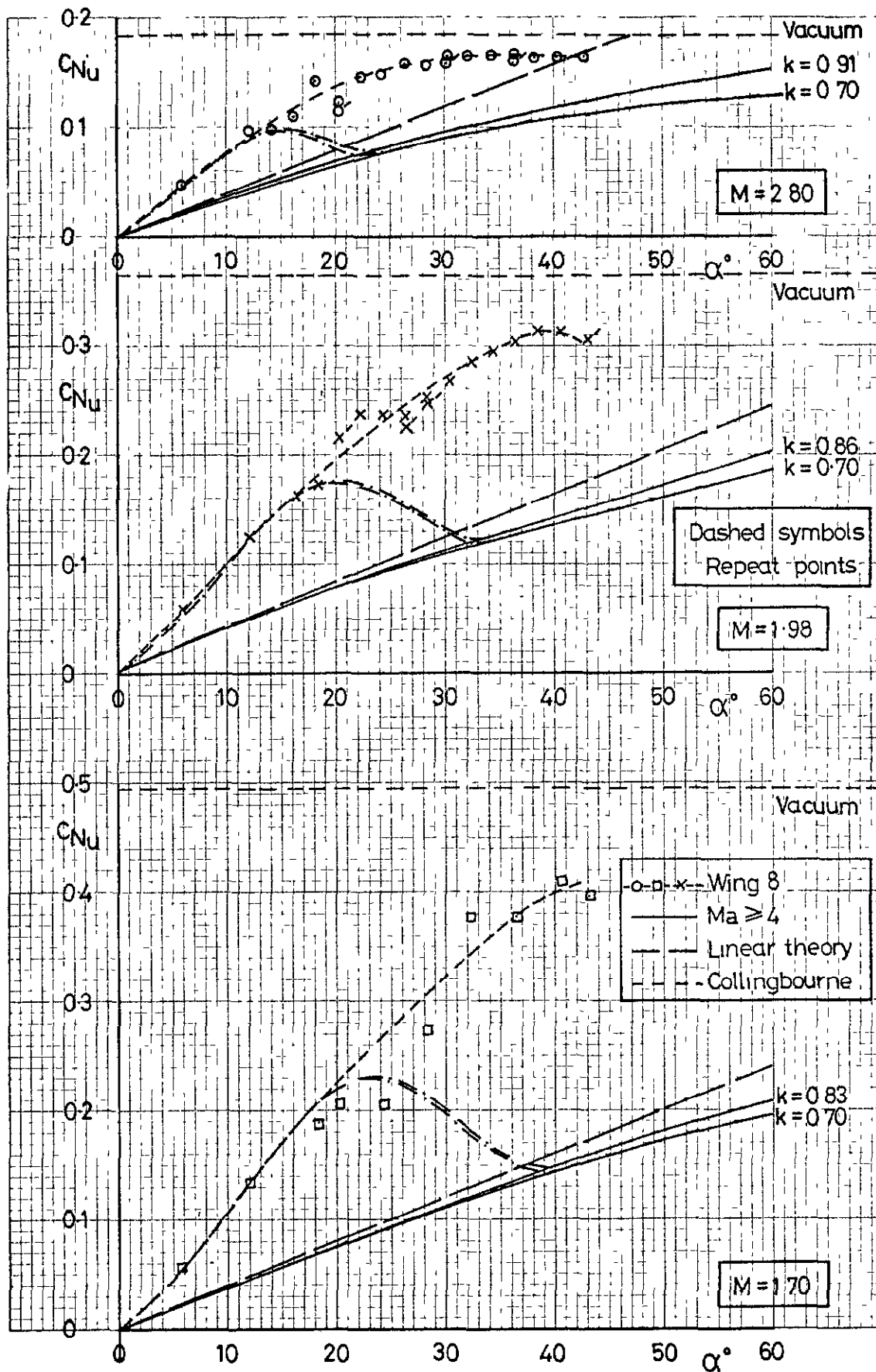


FIG. 7a. UPPER SURFACE NORMAL FORCE AGAINST INCIDENCE.
WING 8

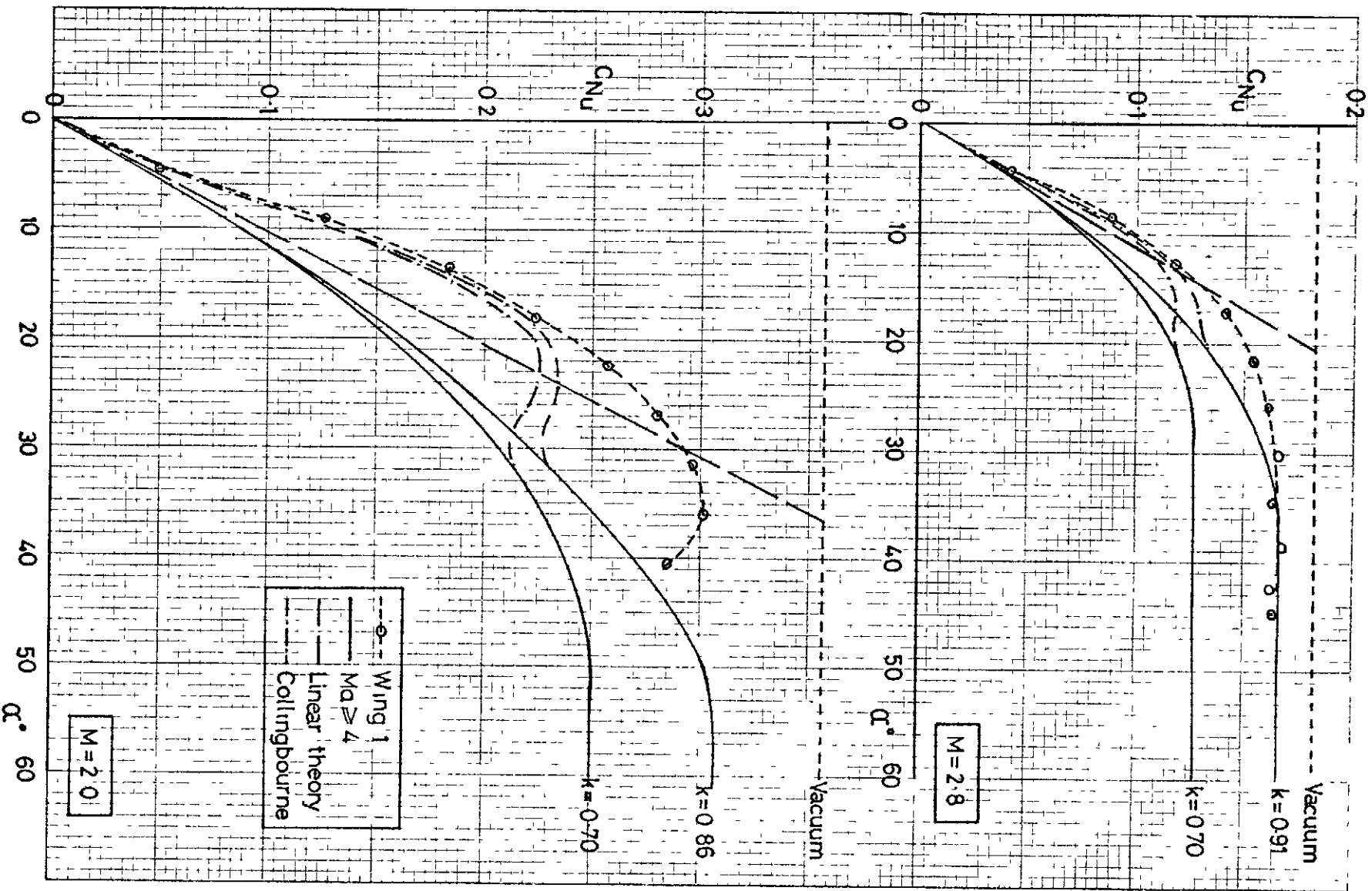


FIG 7b. UPPER SURFACE NORMAL FORCE AGAINST INCIDENCE
WING 1.

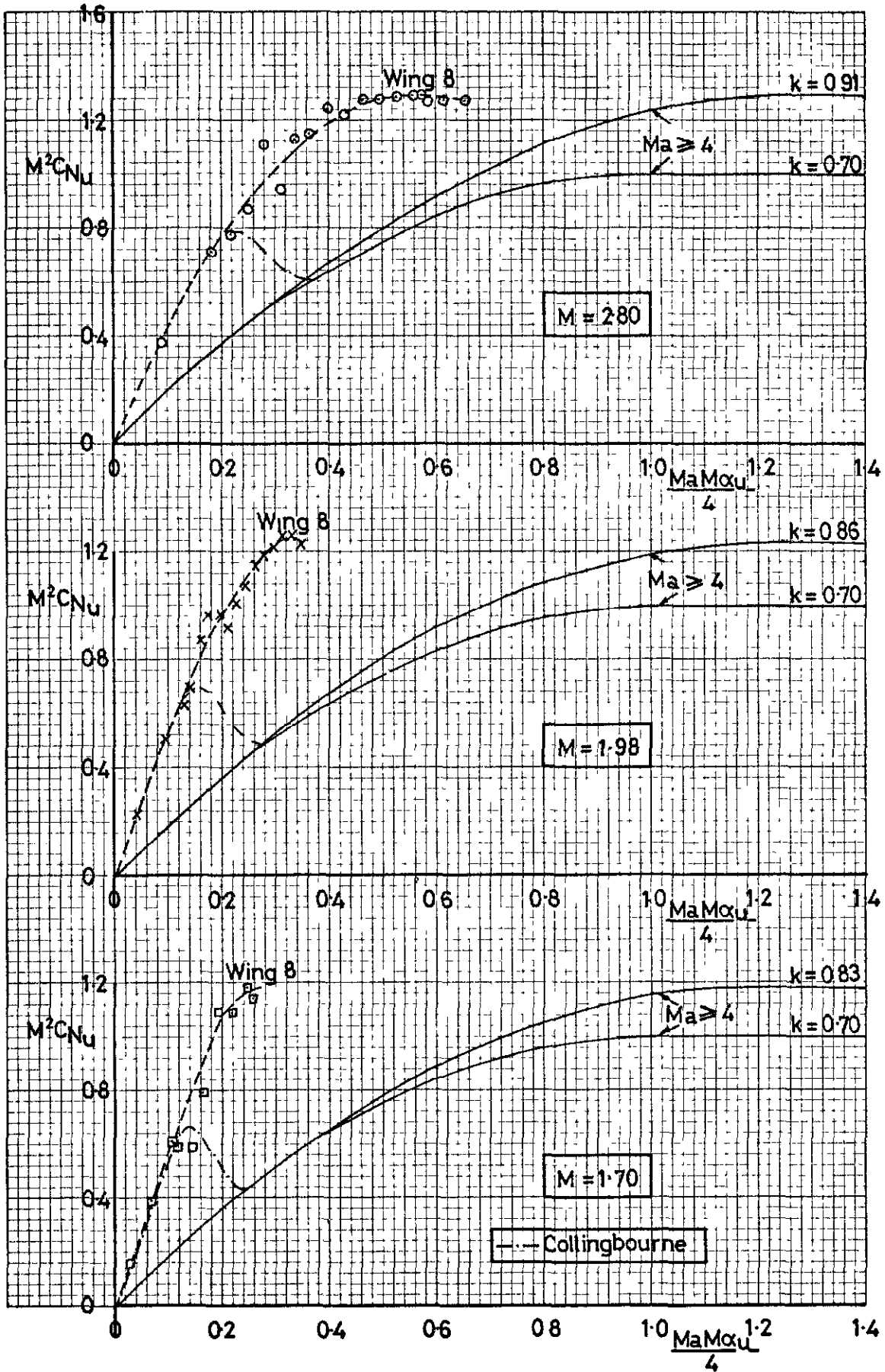


FIG. 8a $M^2 C_{N_u}$ AGAINST $\frac{Ma M \alpha_u}{4}$ WING 8.

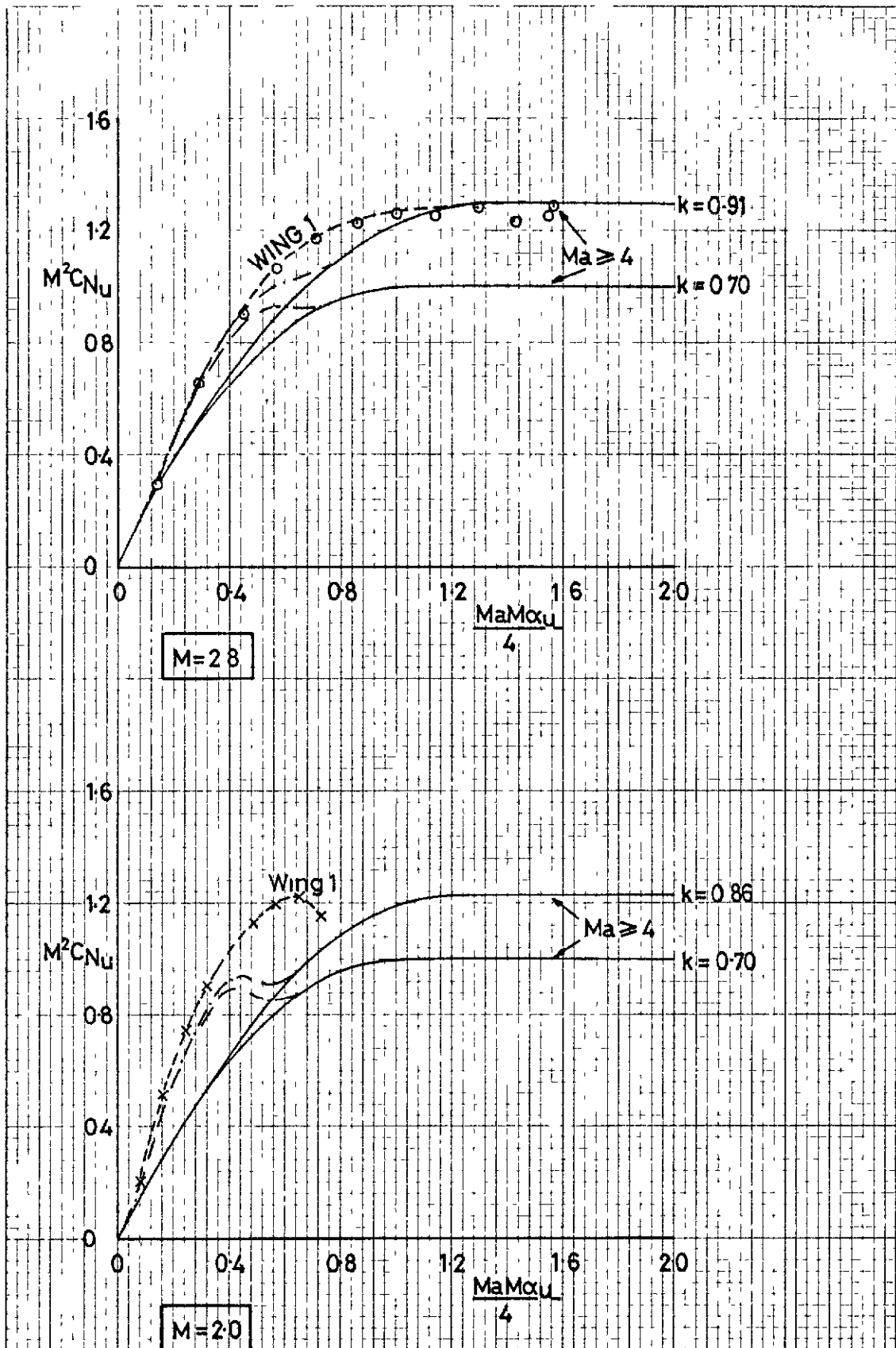


FIG. 8b $M^2 C_{Nu}$ AGAINST $\frac{Ma M \alpha_u}{4}$ WING 1

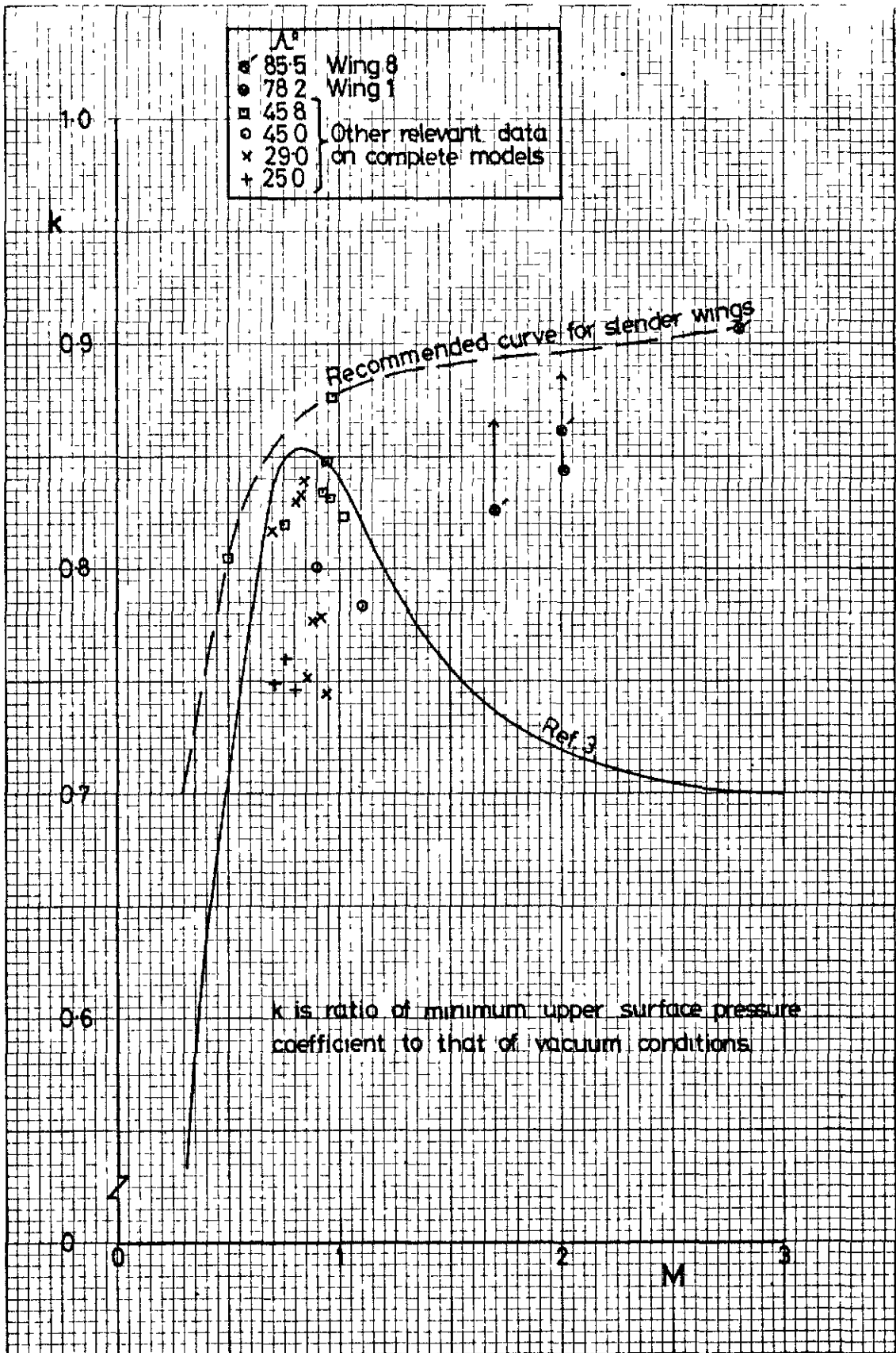


FIG. 9. RELATIONSHIP BETWEEN k AND M.

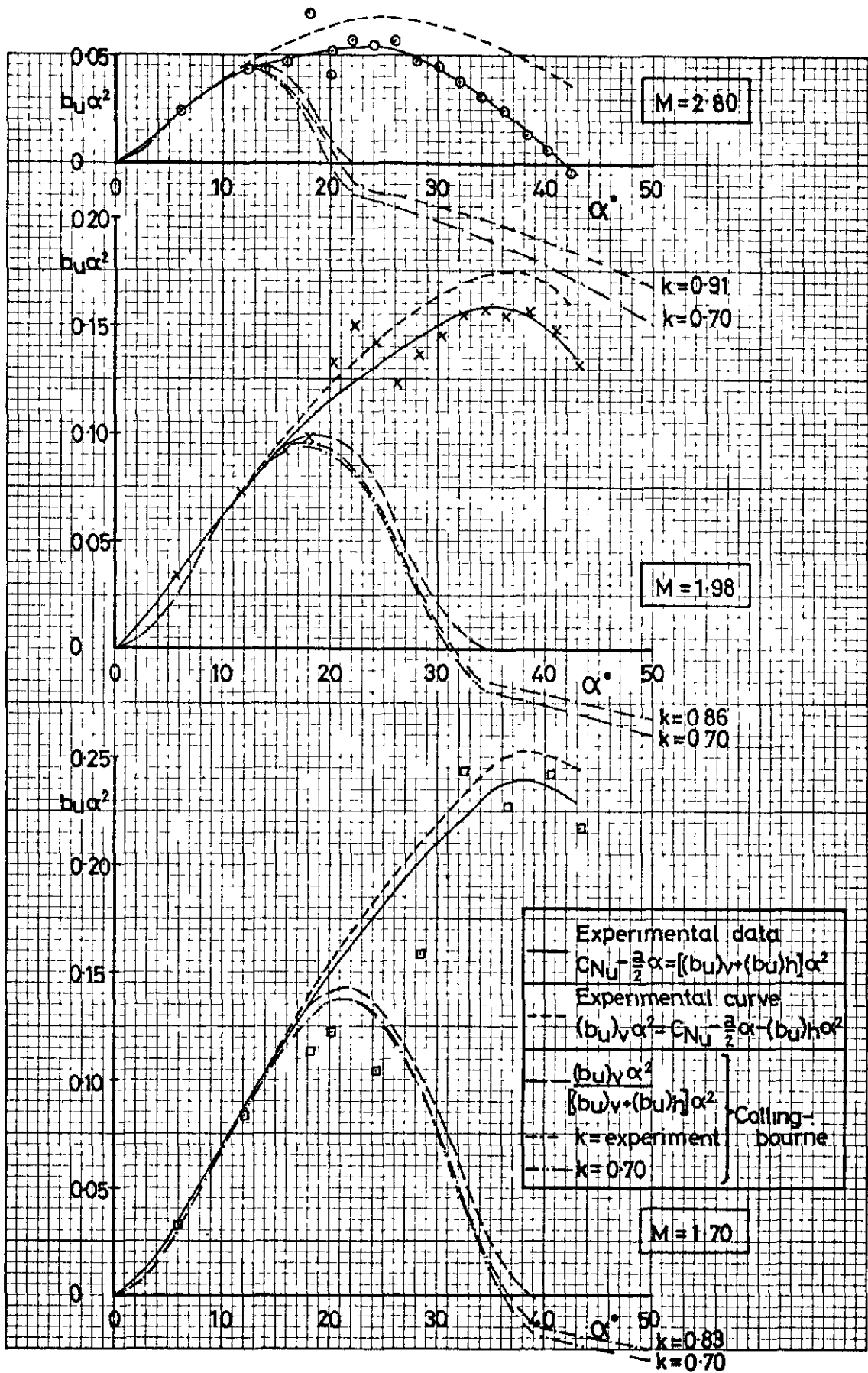


FIG 10a. UPPER SURFACE NON-LINEAR NORMAL FORCE AGAINST INCIDENCE WING 8

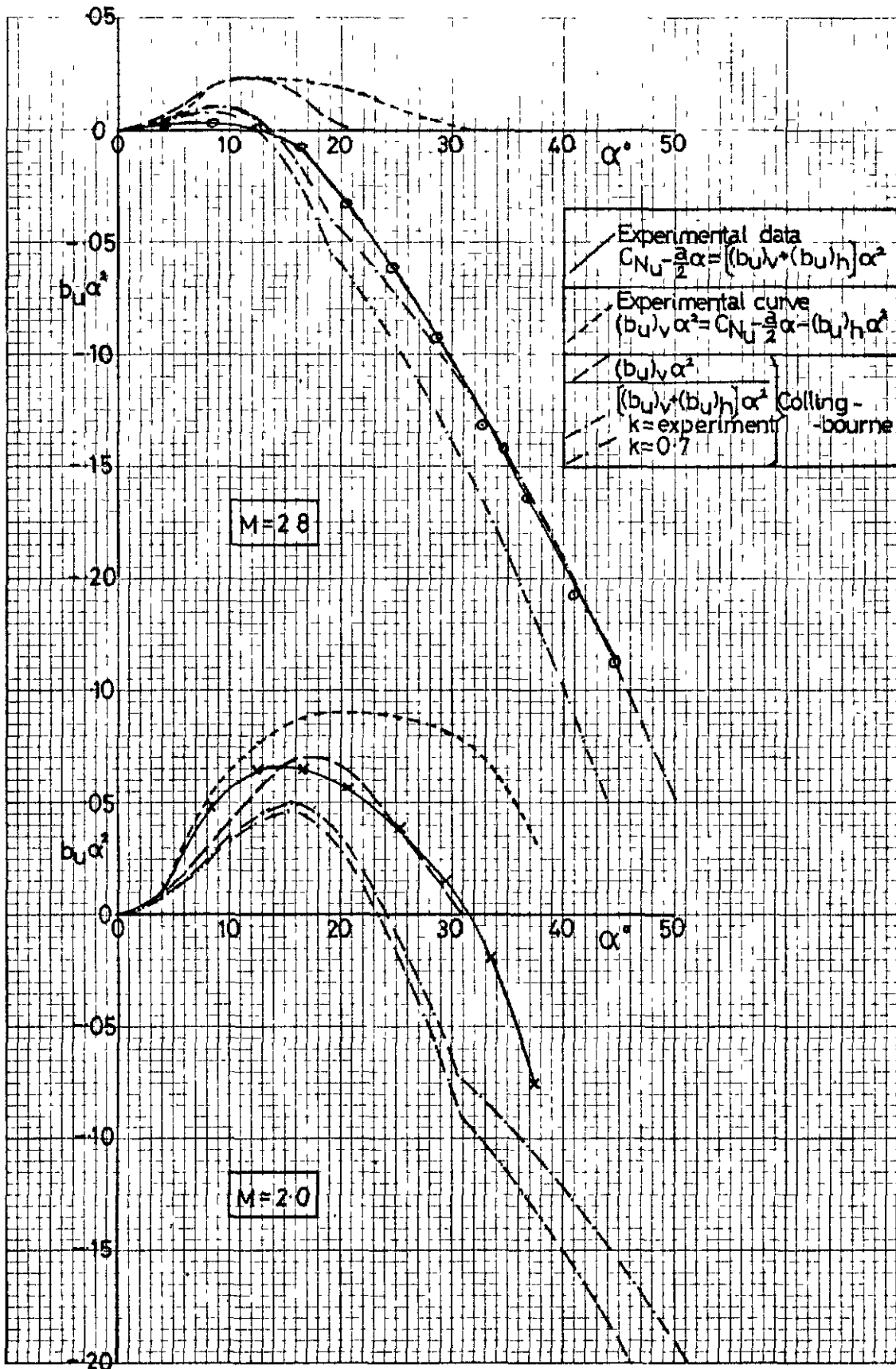


FIG.10b. UPPER SURFACE NON-LINEAR NORMAL FORCE AGAINST INCIDENCE. WING 1.

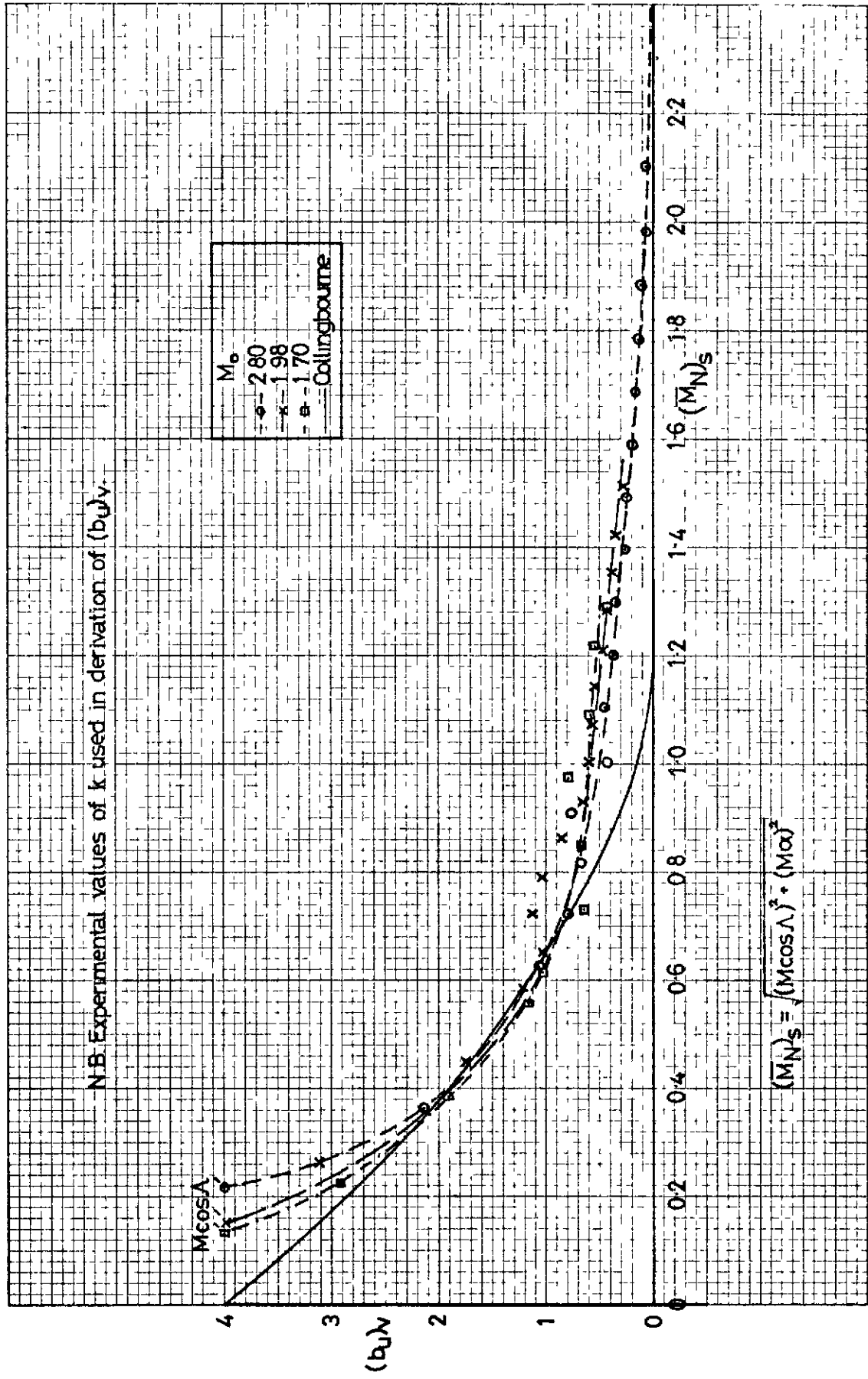


FIG.11a. LEADING EDGE VORTEX FACTOR AGAINST $(\bar{M}_N)_s$ WING 8.

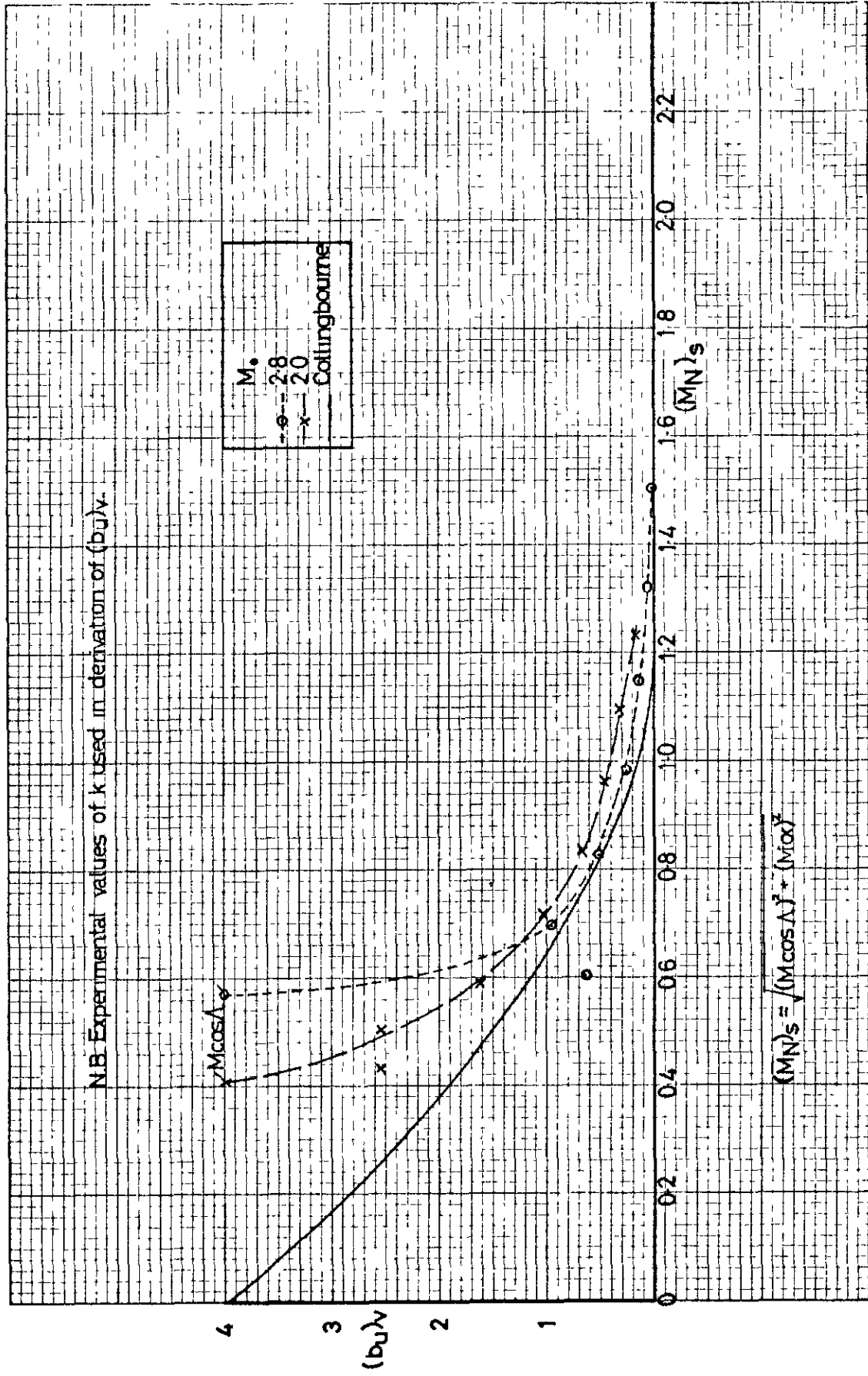


FIG.11b. LEADING EDGE VORTEX FACTOR AGAINST $(M_N)_s$ WING 1.

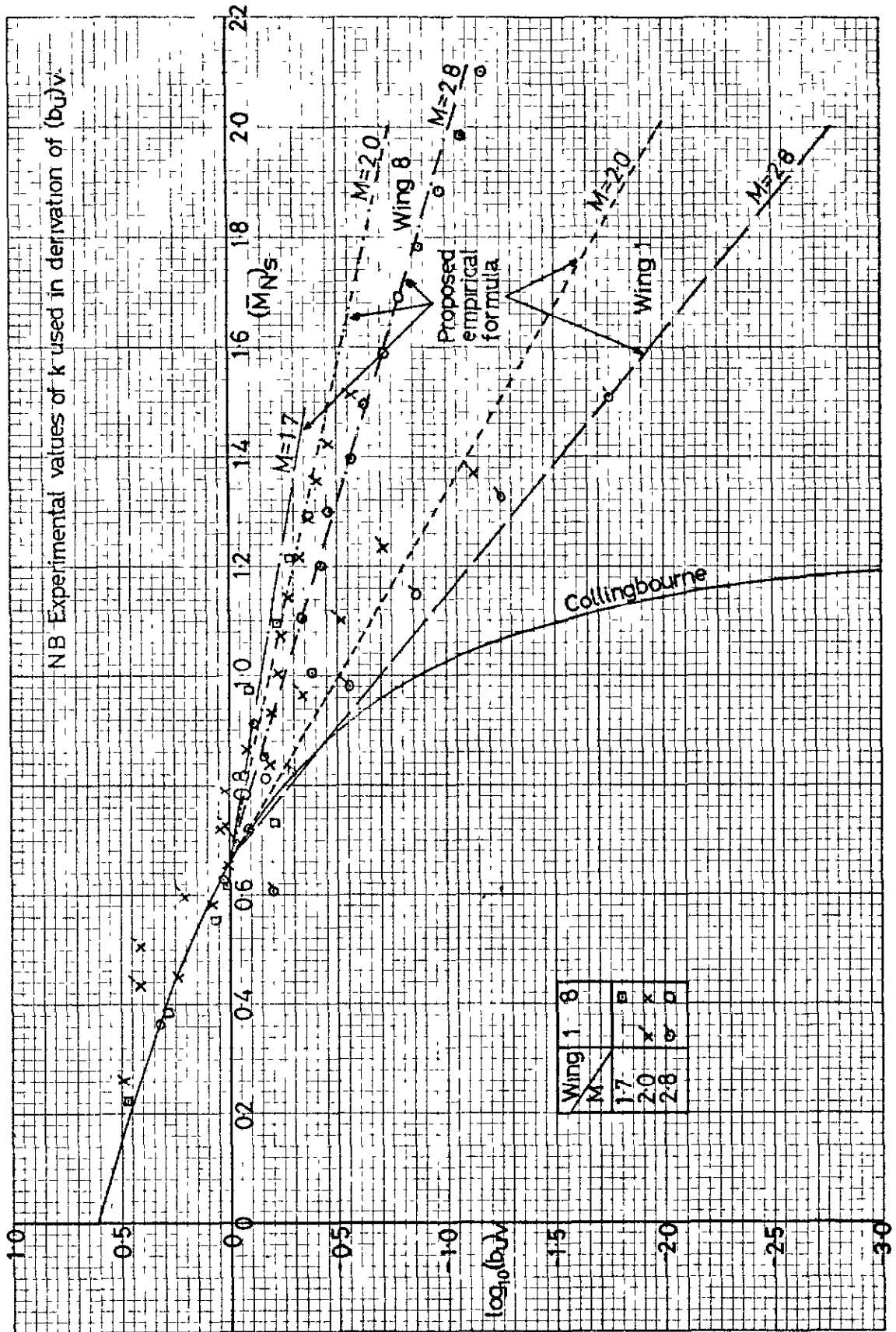


FIG. 12. $\log_{10}(b_u)_v$ AGAINST $(\bar{M}_N)_s$

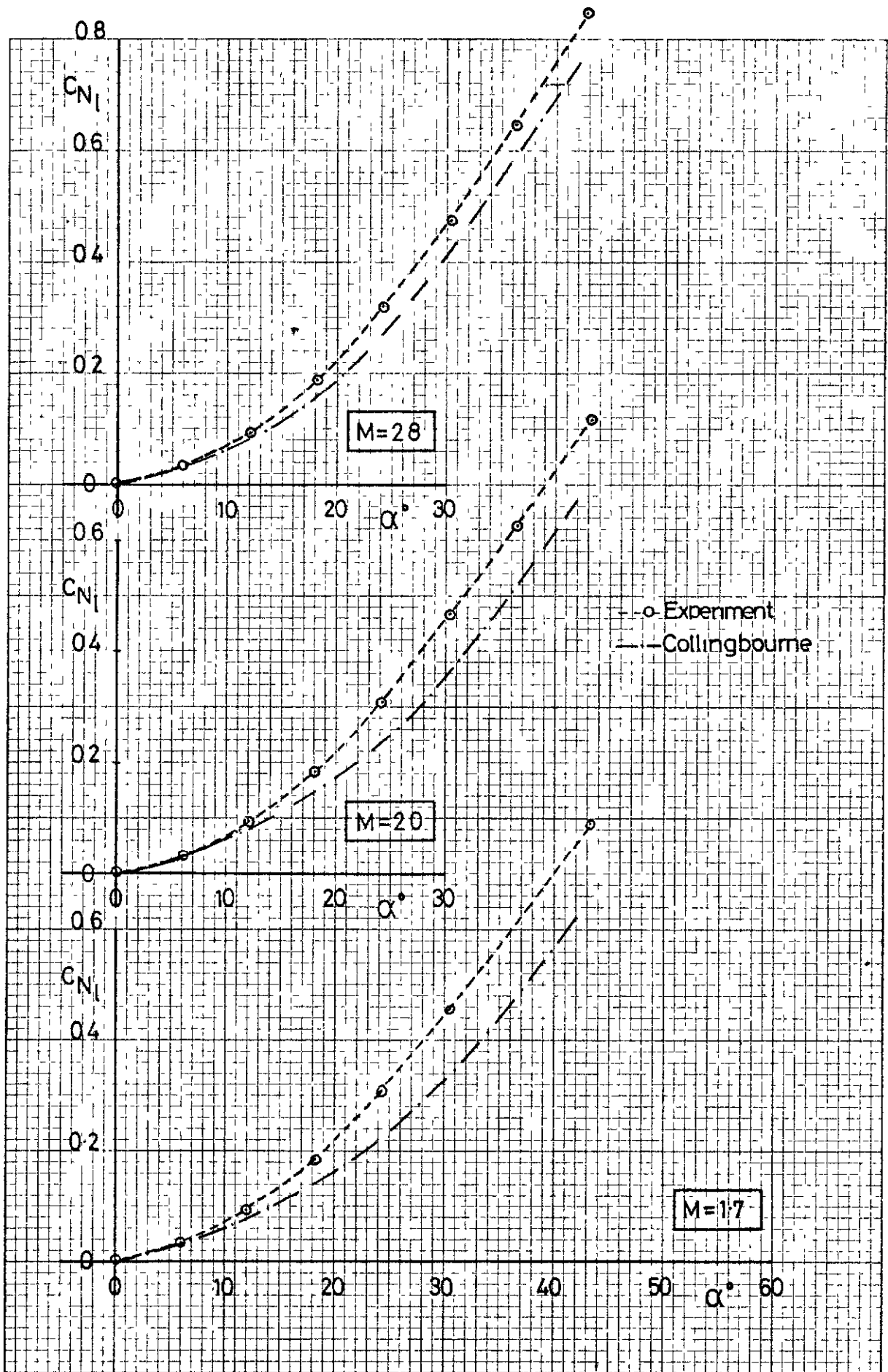


FIG.13a. LOWER SURFACE NORMAL FORCE AGAINST INCIDENCE WING 8

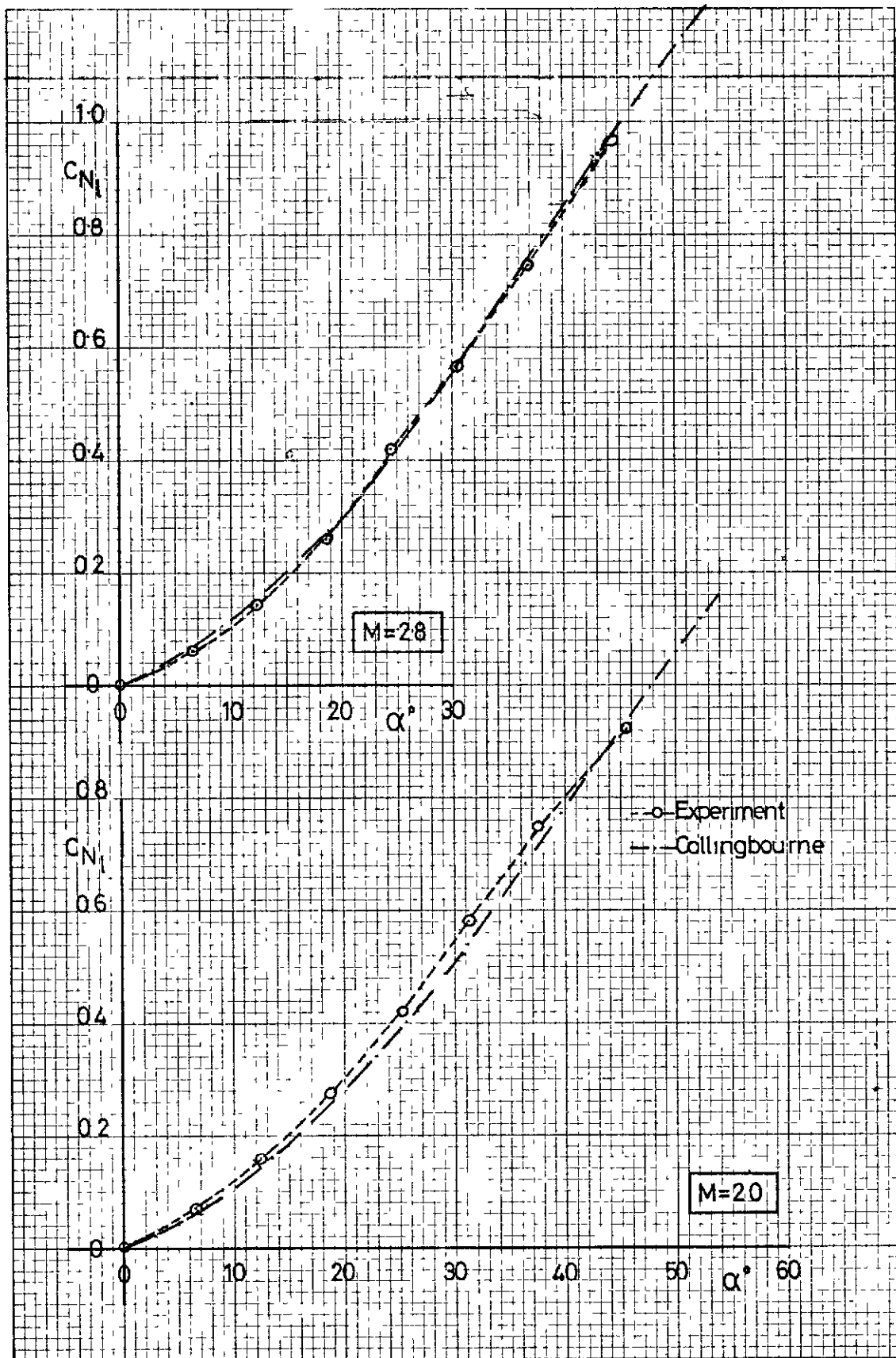


FIG13b LOWER SURFACE NORMAL FORCE AGAINST INCIDENCE
WING 1

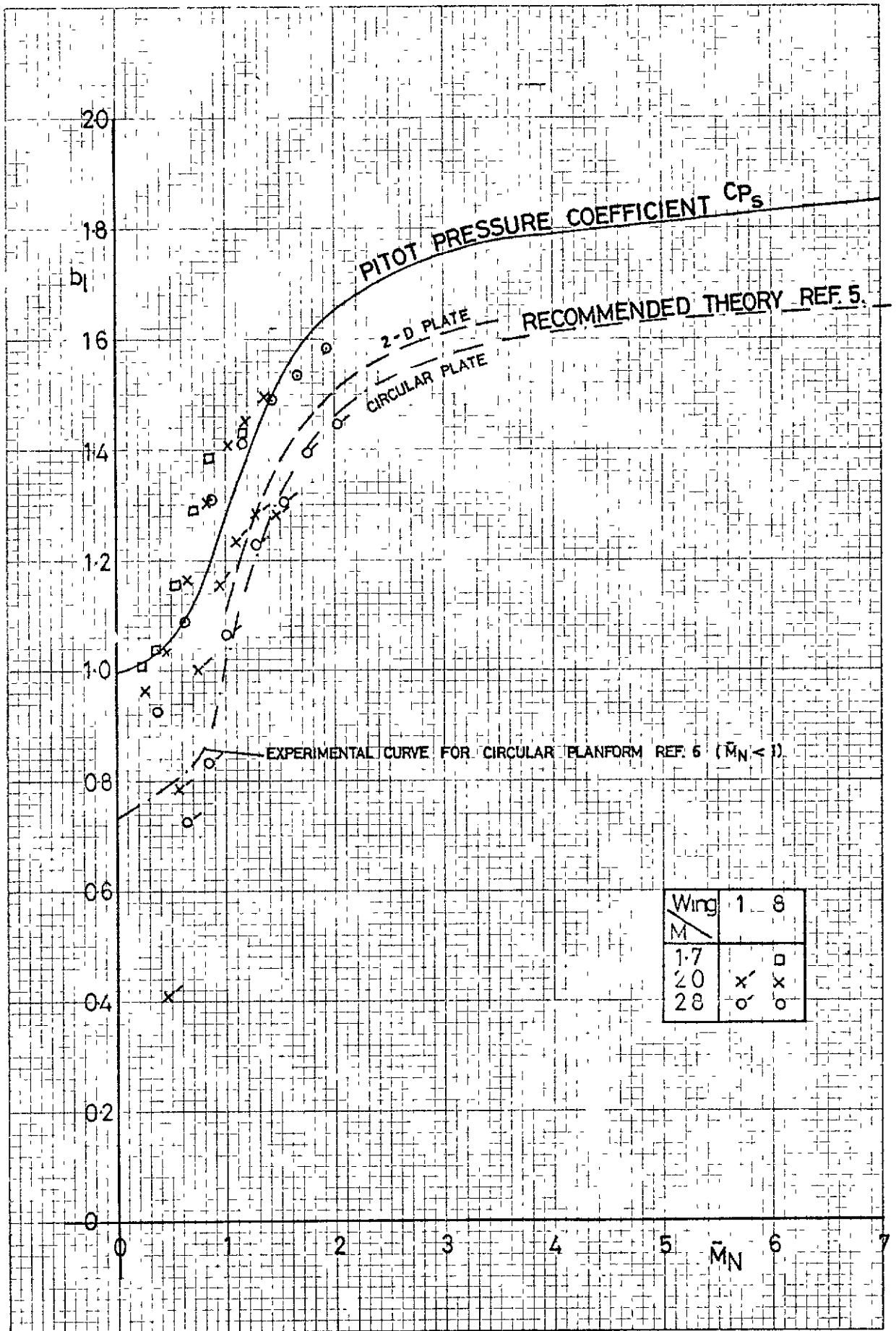
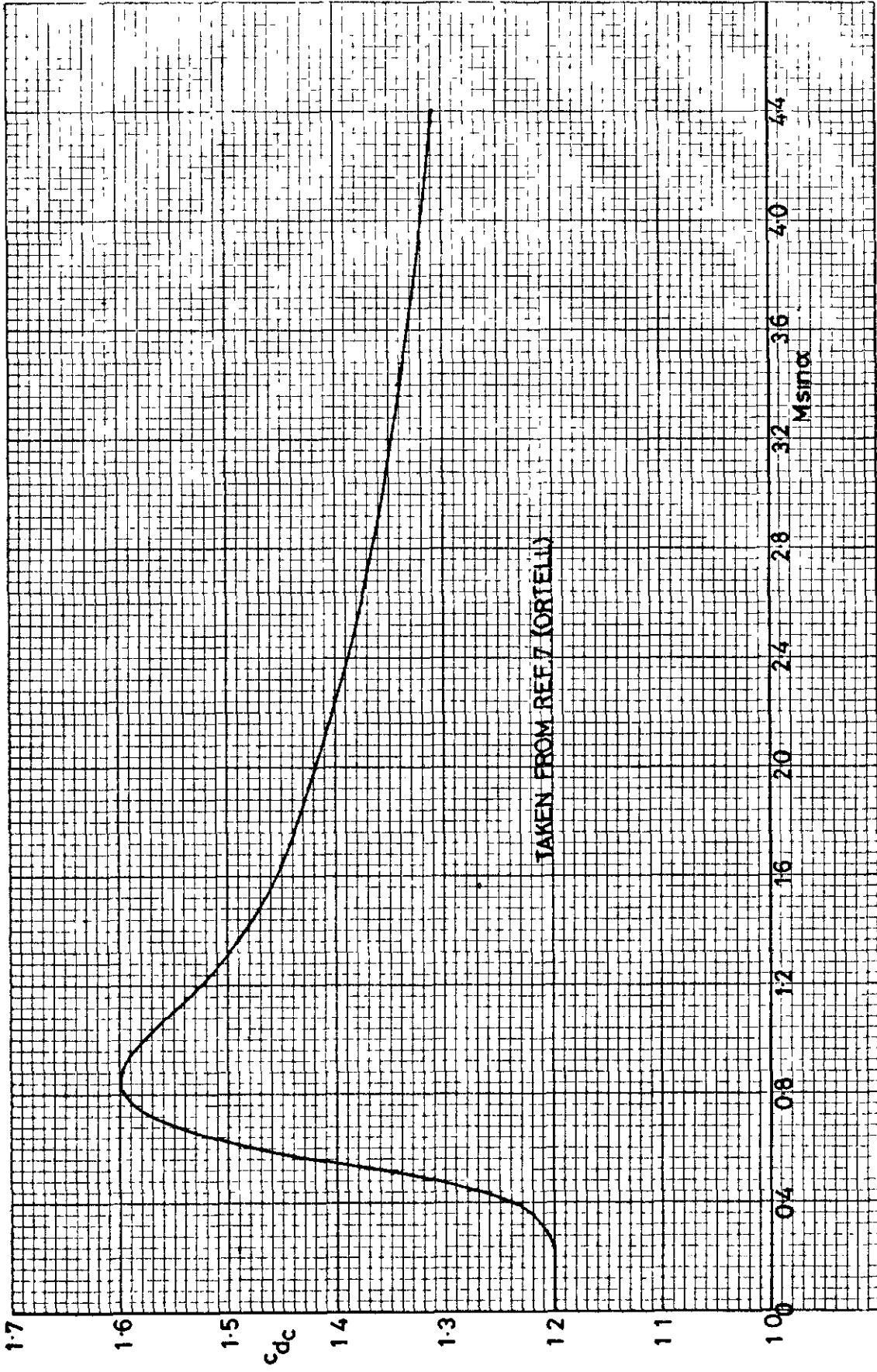


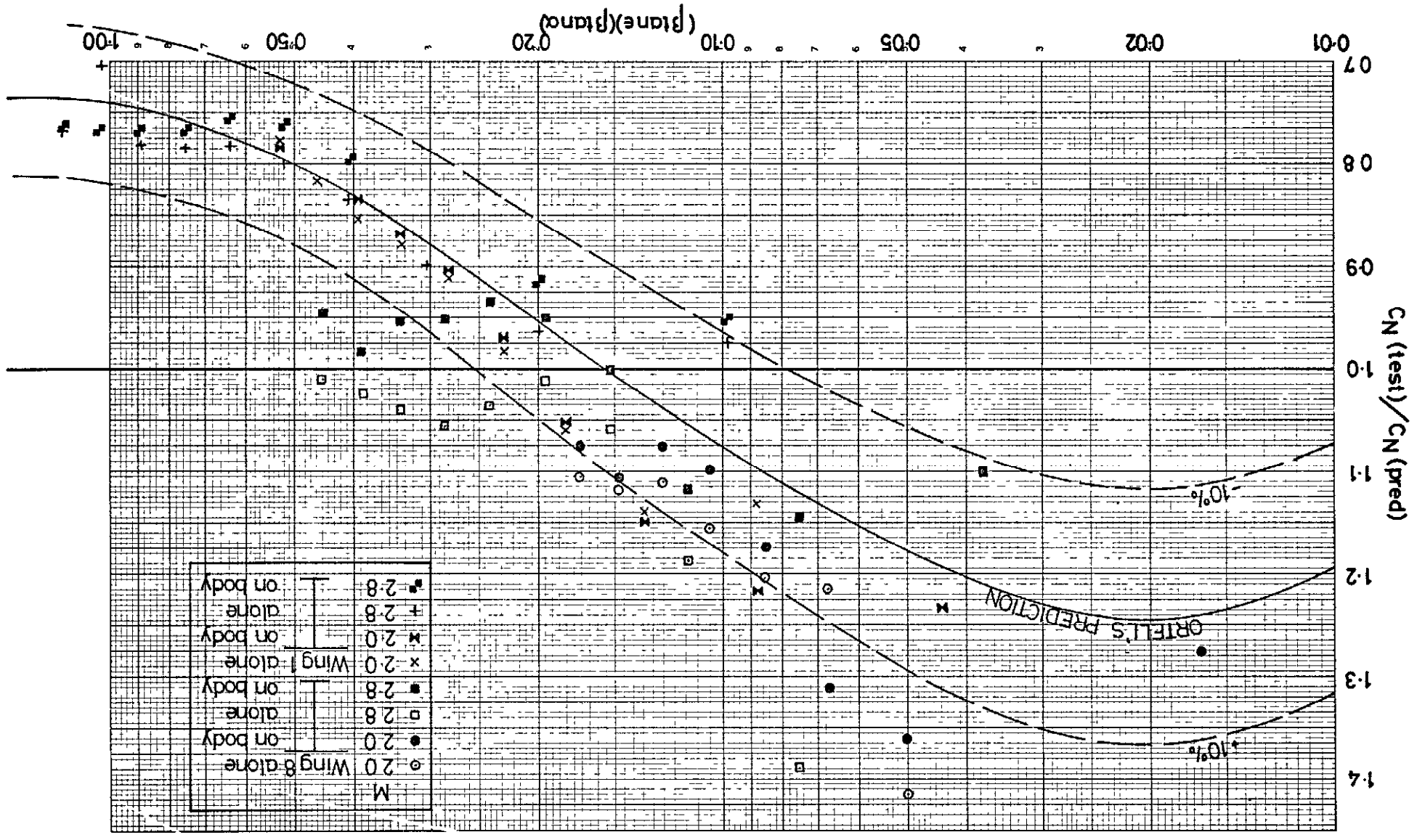
FIG. 14. LOWER SURFACE NON-LINEAR FACTOR b_l AGAINST \bar{M}_N



TAKEN FROM REF. 7 (ORTELL)

FIG.15 CIRCULAR CYLINDER DRAG COEFFICIENT FOR VISCOUS CROSS-FLOW CALCULATIONS

FIG 16. COMPARISON OF CURRENT DATA WITH ORTELL'S PREDICTION (REF 7)



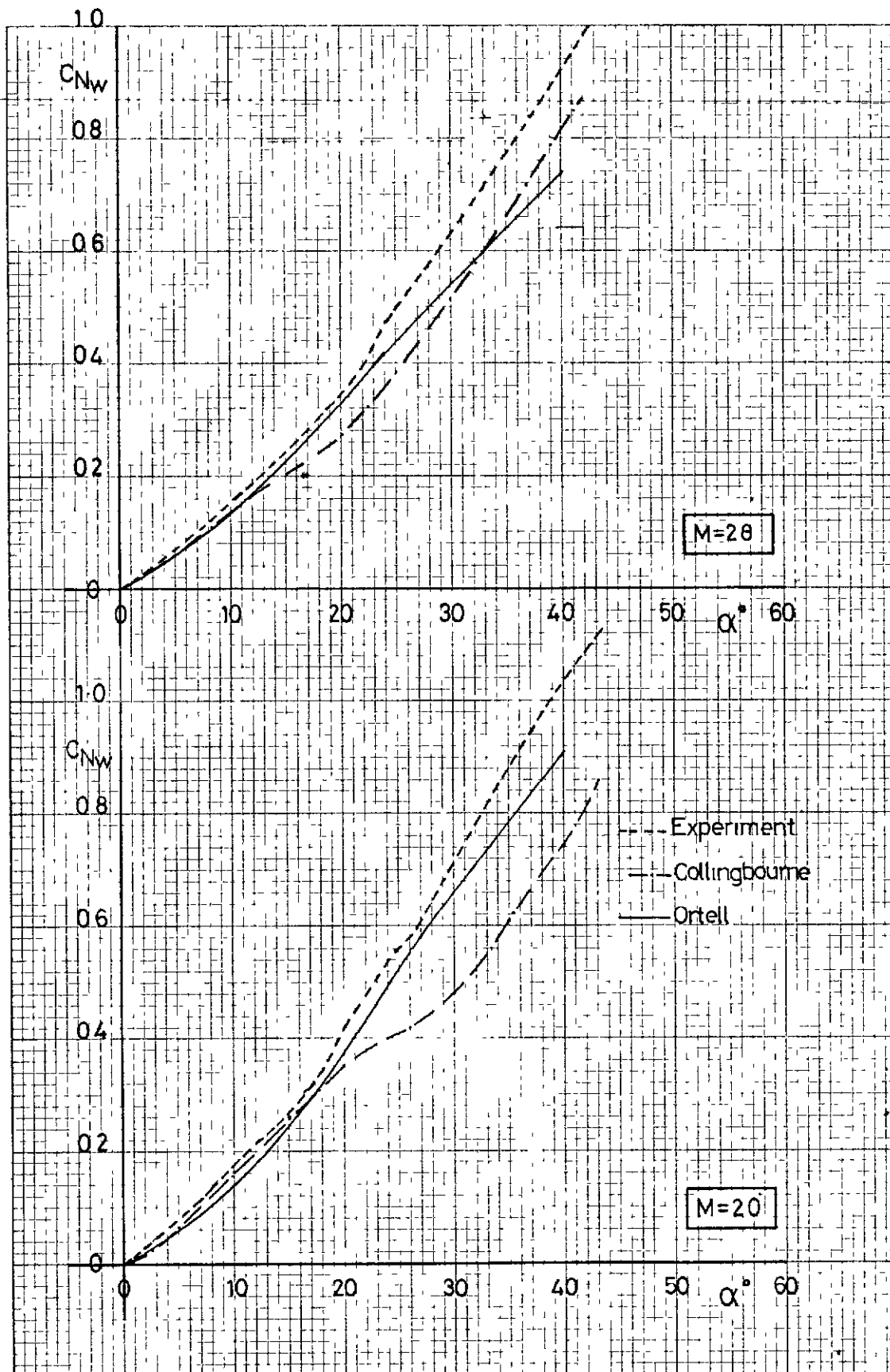


FIG.17a. NORMAL FORCE AGAINST INCIDENCE WING 8
COMPARISON OF EXPERIMENT AND THEORY

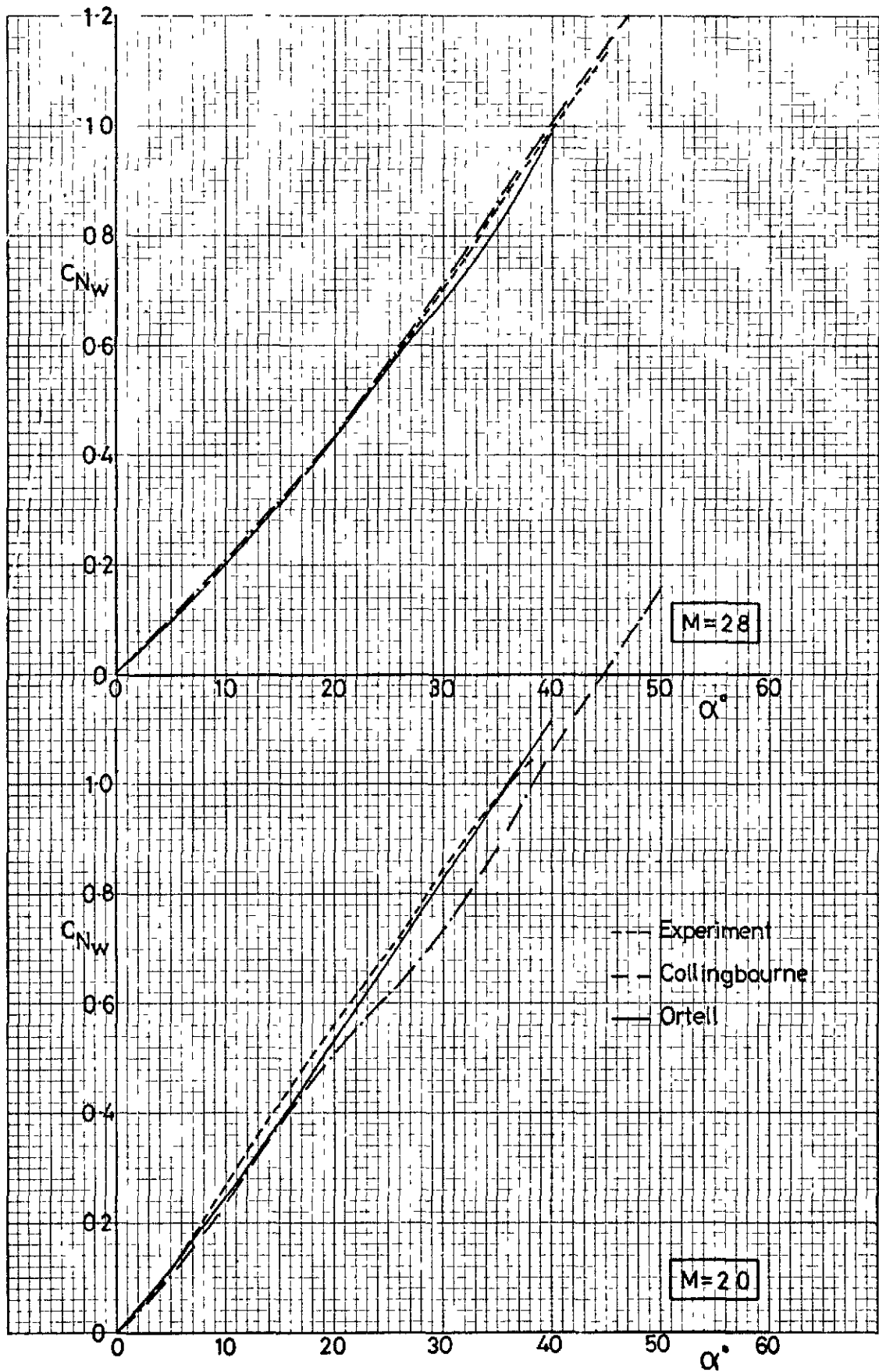


FIG 17b. NORMAL FORCE AGAINST INCIDENCE WING 1
COMPARISON OF EXPERIMENT AND THEORY

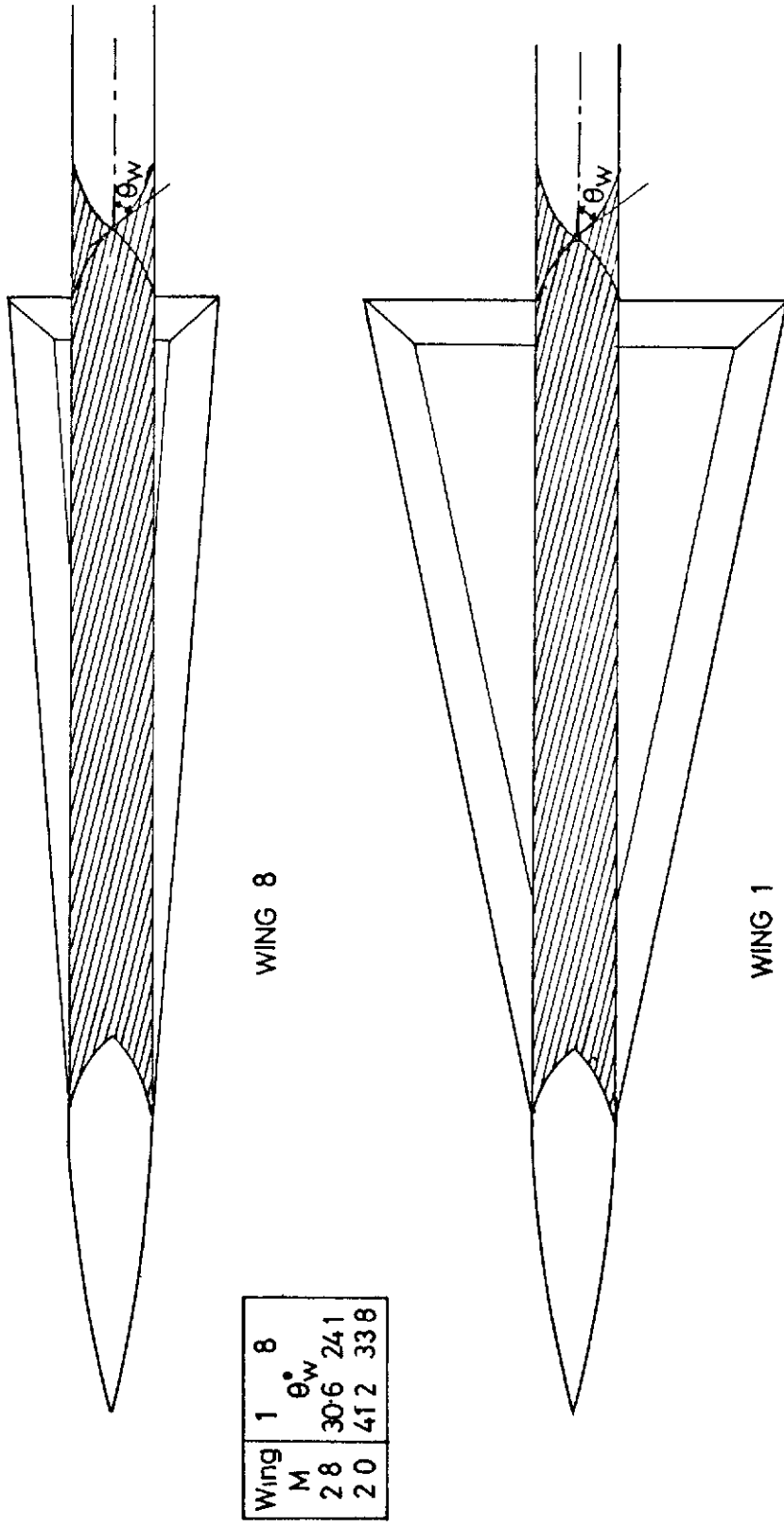


FIG. 18. REGION OF BODY INFLUENCED BY WINGS

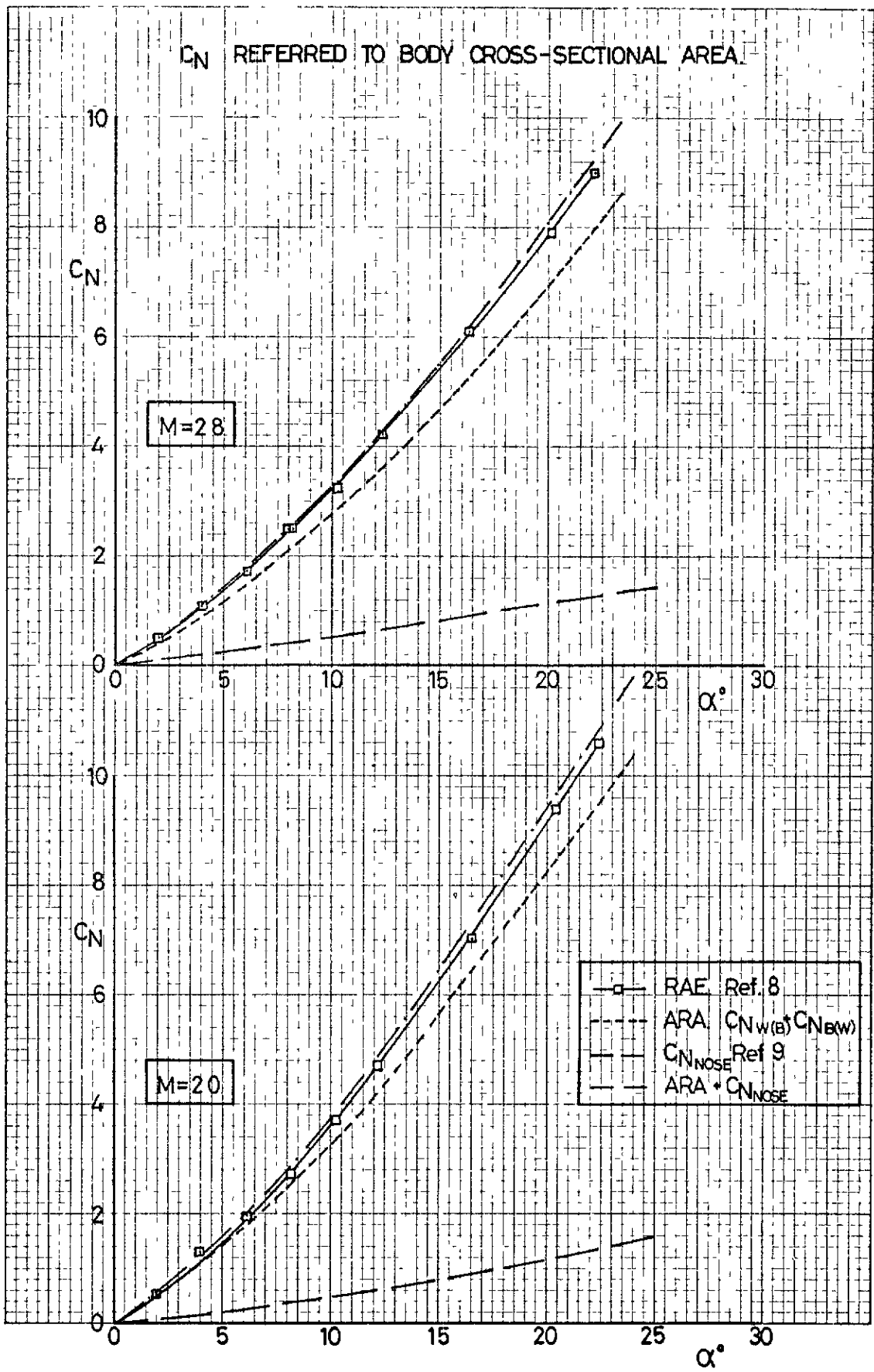


FIG. 19a. COMPARISON WITH BALANCE MEASUREMENTS
WING 8 ON BODY

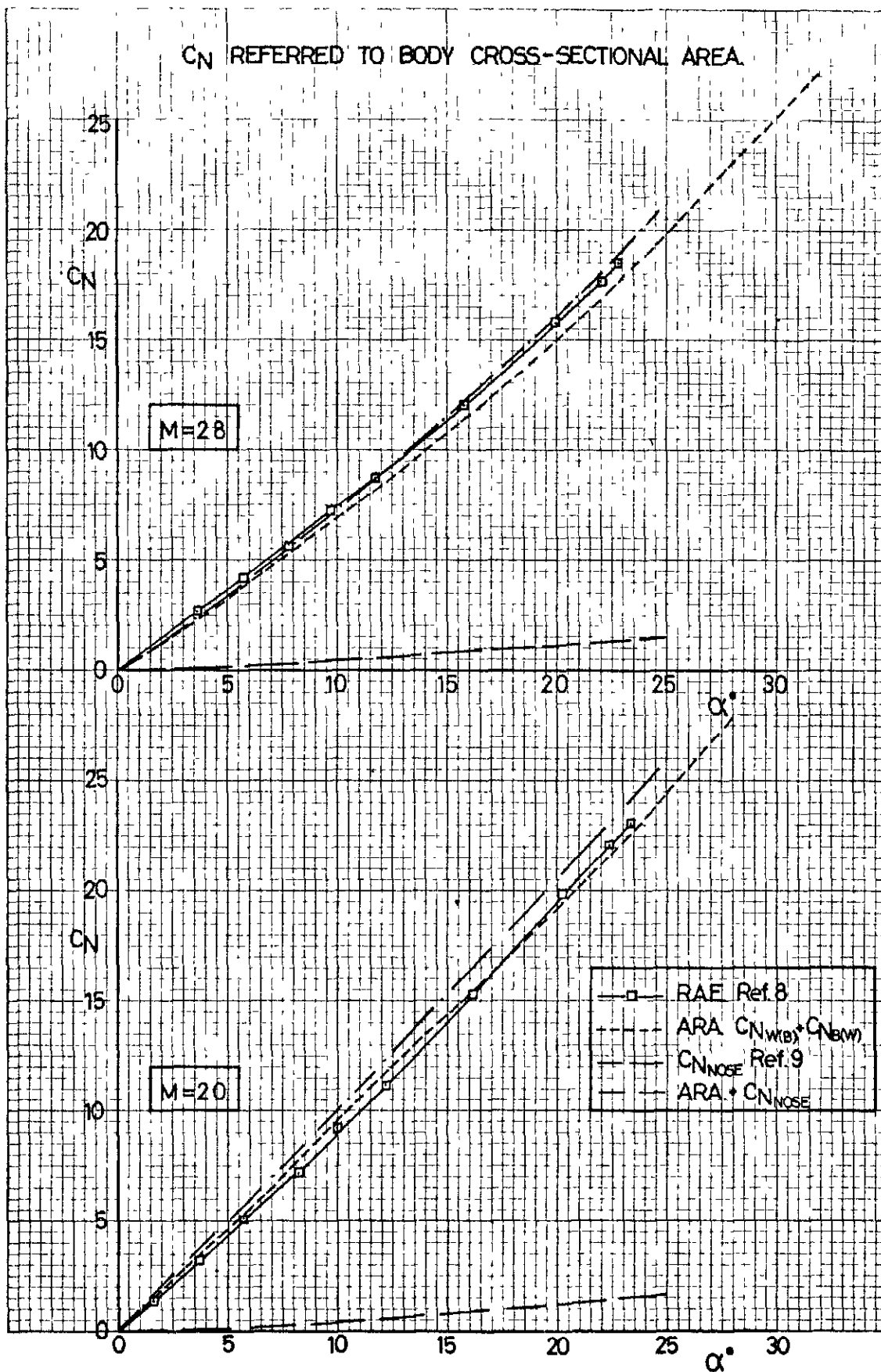


FIG. 19b. COMPARISON WITH BALANCE MEASUREMENTS
WING 1 ON BODY

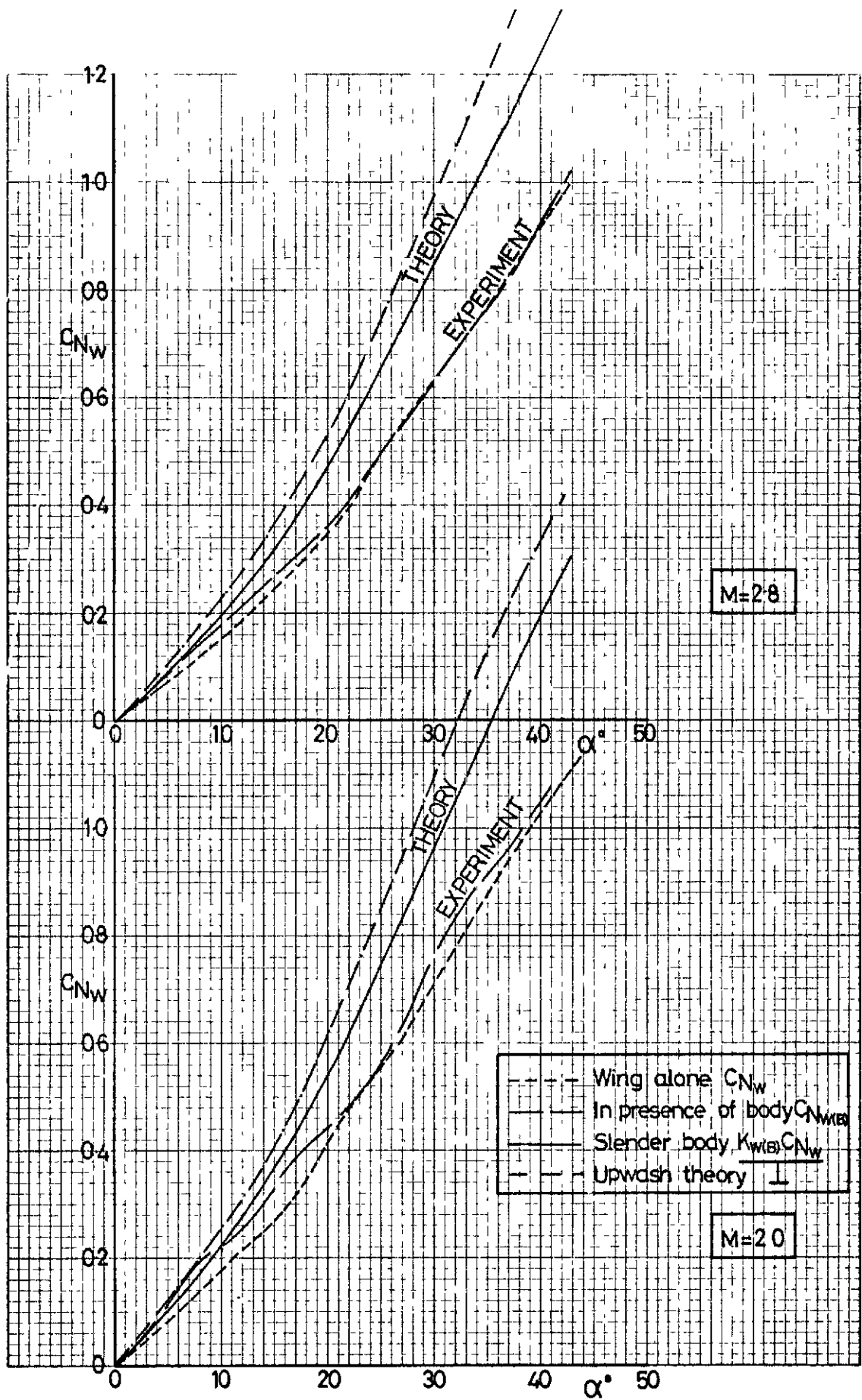


FIG. 20a INTERFERENCE FROM BODY ON WING 8
COMPARISON OF EXPERIMENT AND THEORY.

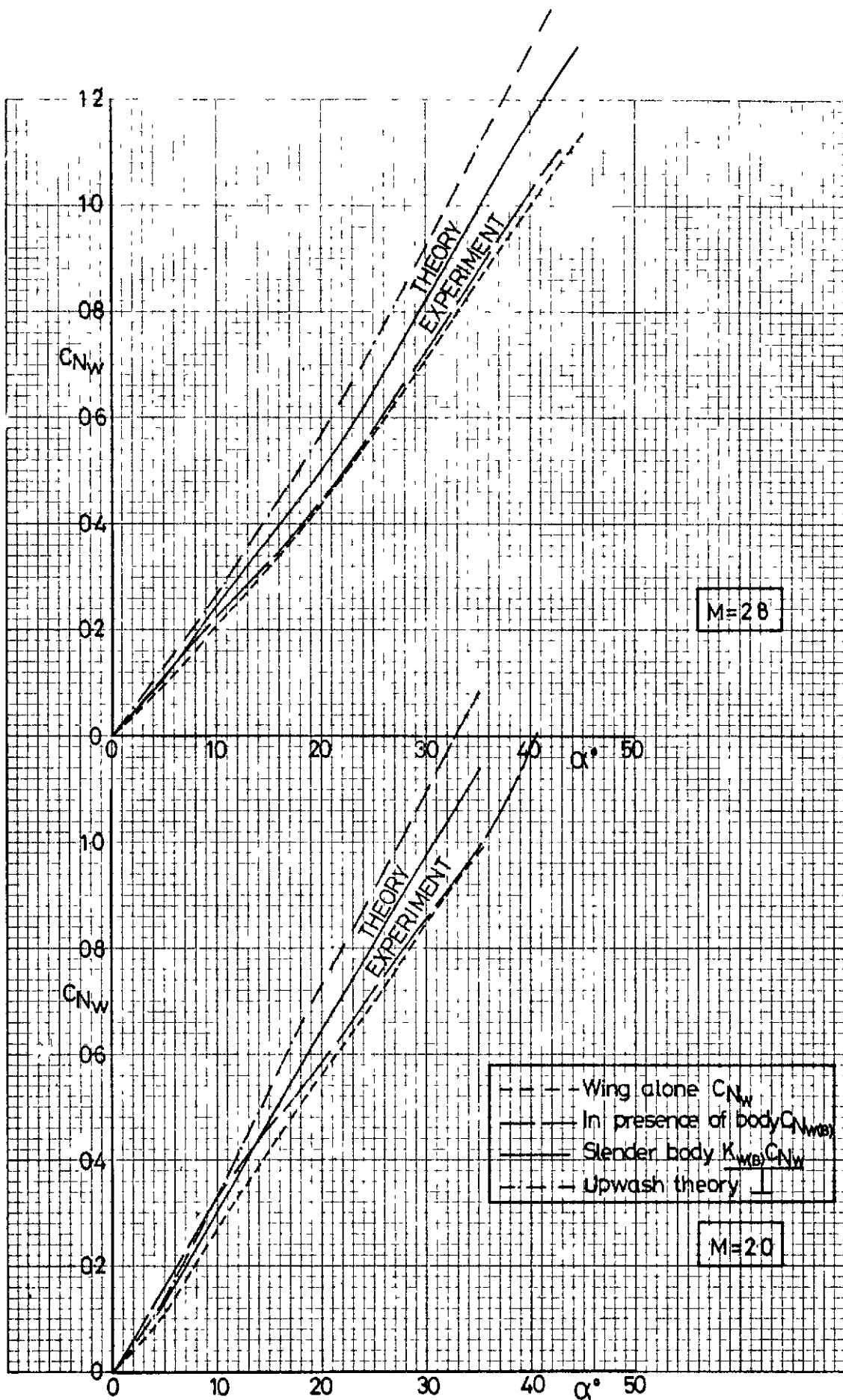


FIG 20b. INTERFERENCE FROM BODY ON WING 1
COMPARISON OF EXPERIMENT AND THEORY

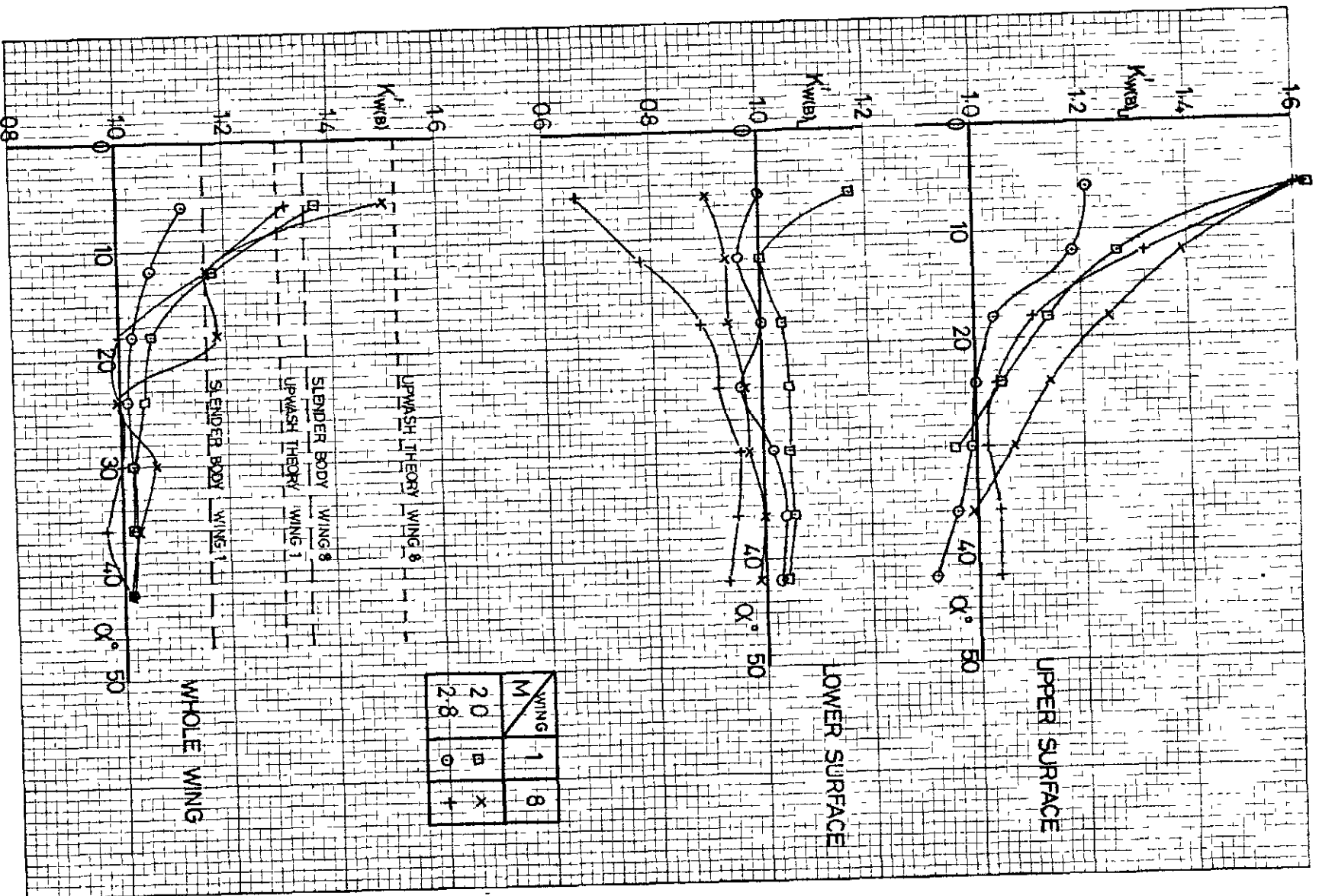


FIG. 21 EXPERIMENTAL BODY ON WING INTERFERENCE FACTOR FOR EACH SURFACE AND WHOLE WING

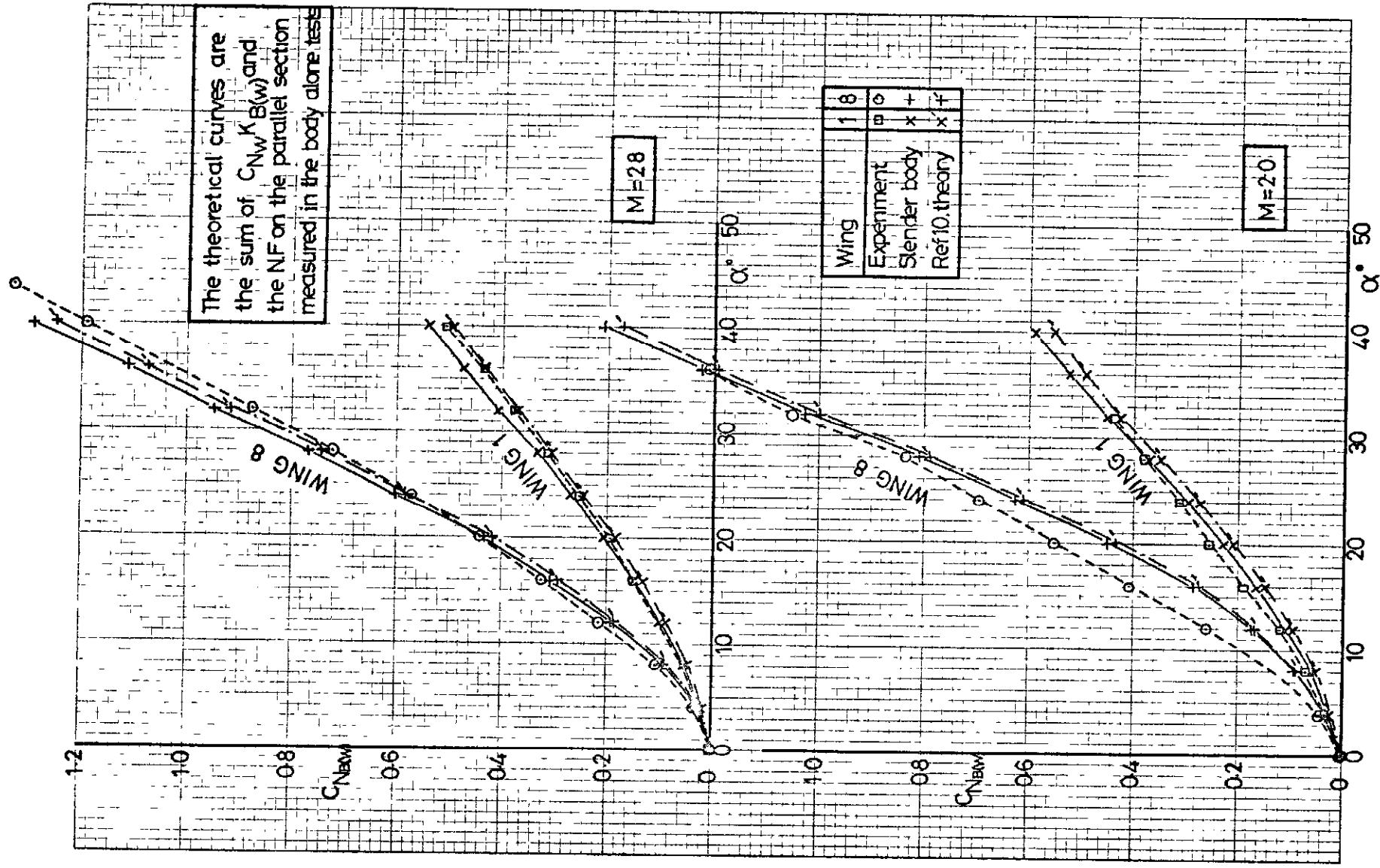


FIG. 22 INTERFERENCE FROM WING ON PARALLEL BODY
COMPARISON OF EXPERIMENT AND THEORY

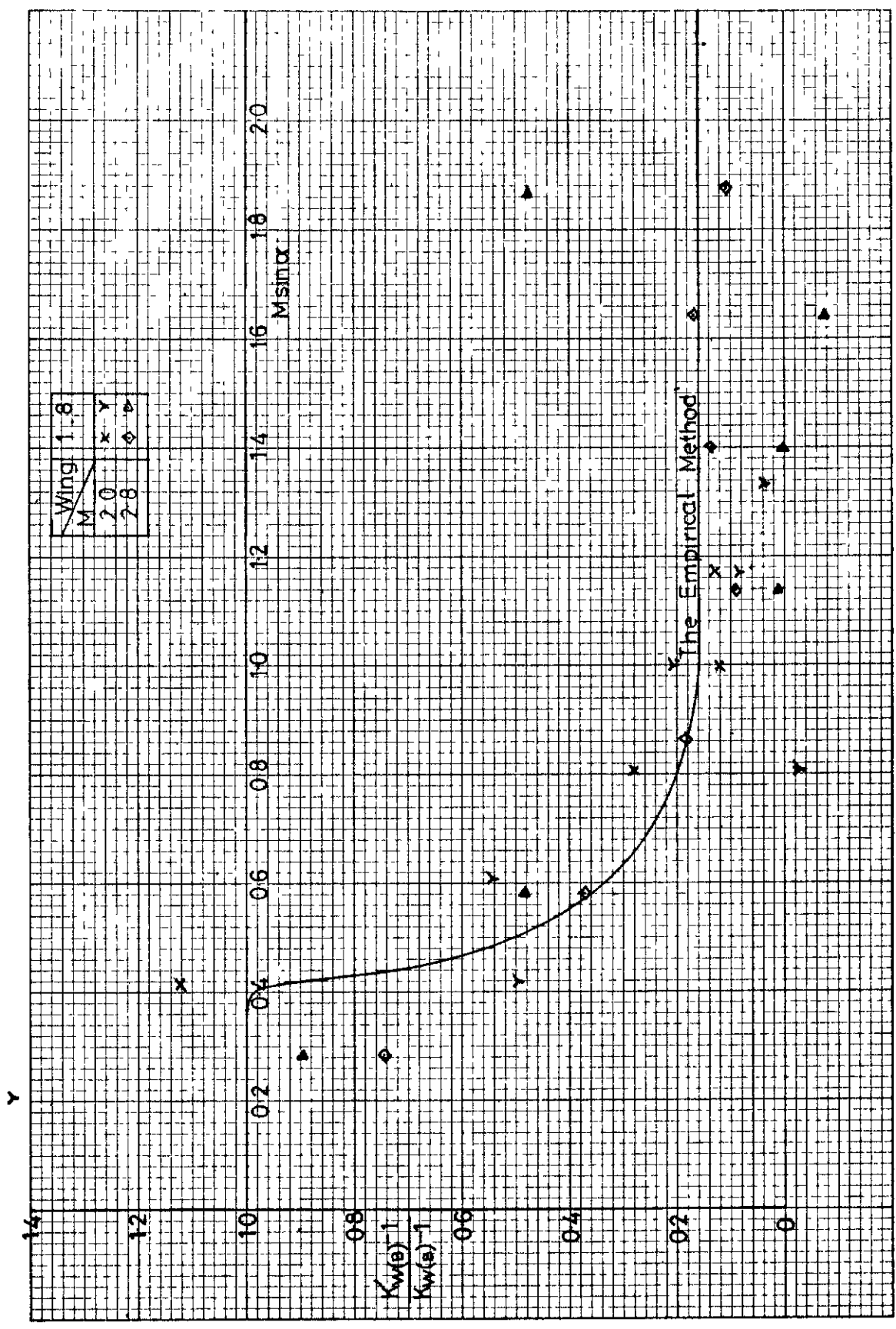


FIG. 23. EFFECT OF CROSS FLOW MACH NUMBER ON INTERFERENCE FROM BODY ON WING.

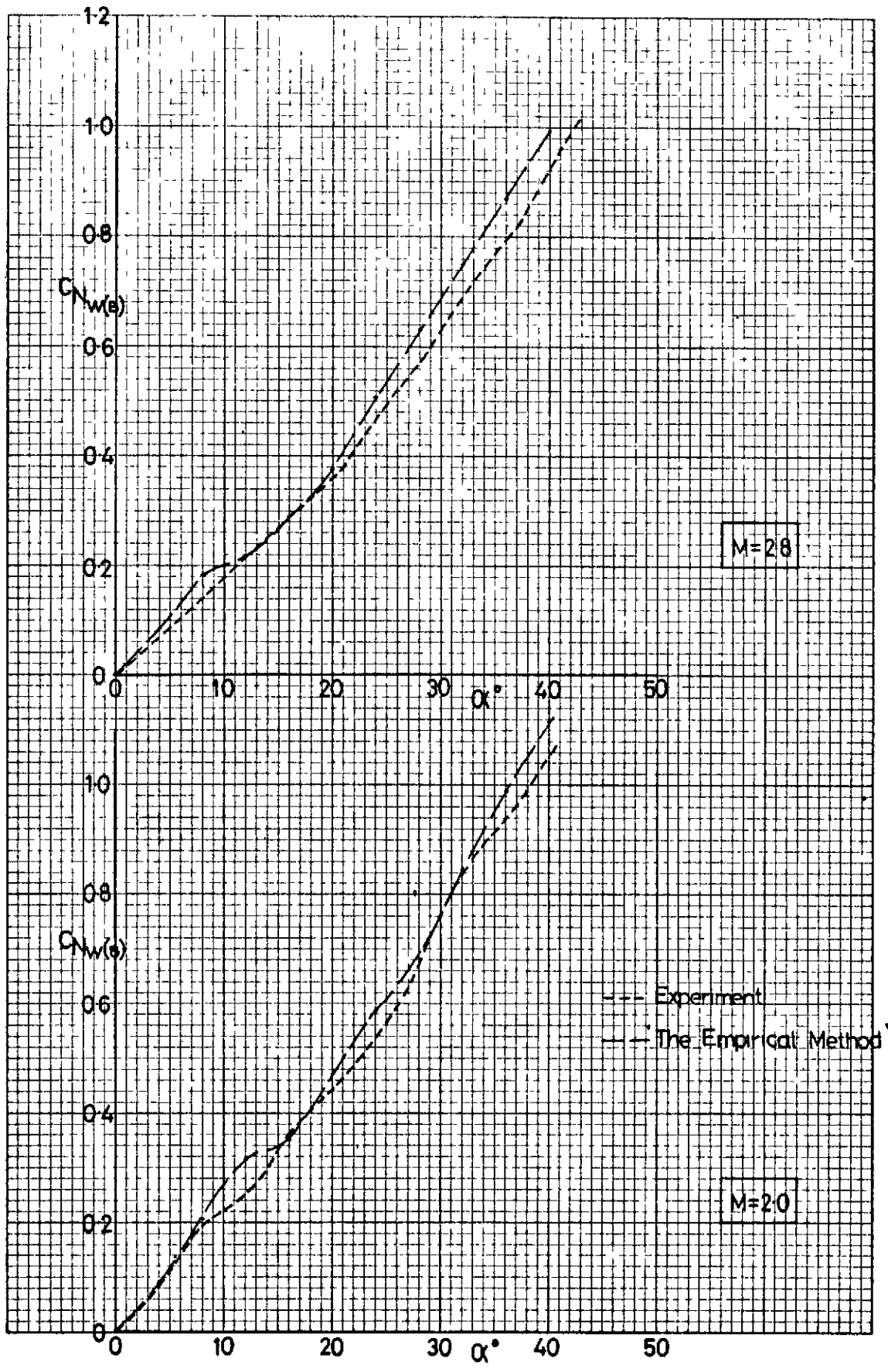


FIG. 24a. NORMAL FORCE ON WING 8 IN PRESENCE OF BODY. COMPARISON OF EXPERIMENT WITH 'EMPIRICAL METHOD.'

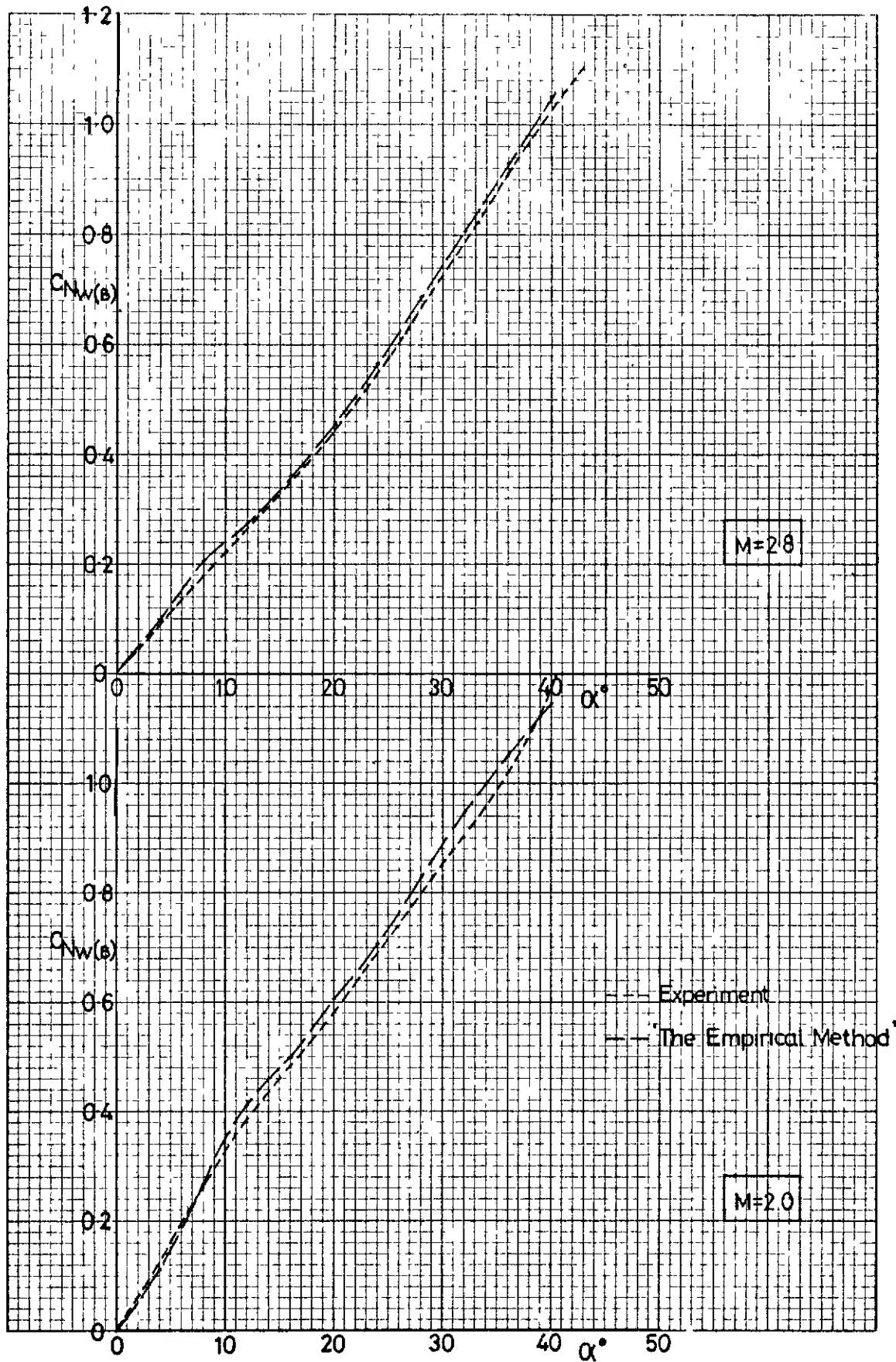


FIG. 24b. NORMAL FORCE ON WING 1 IN PRESENCE OF BODY.
COMPARISON OF EXPERIMENT WITH EMPIRICAL METHOD.

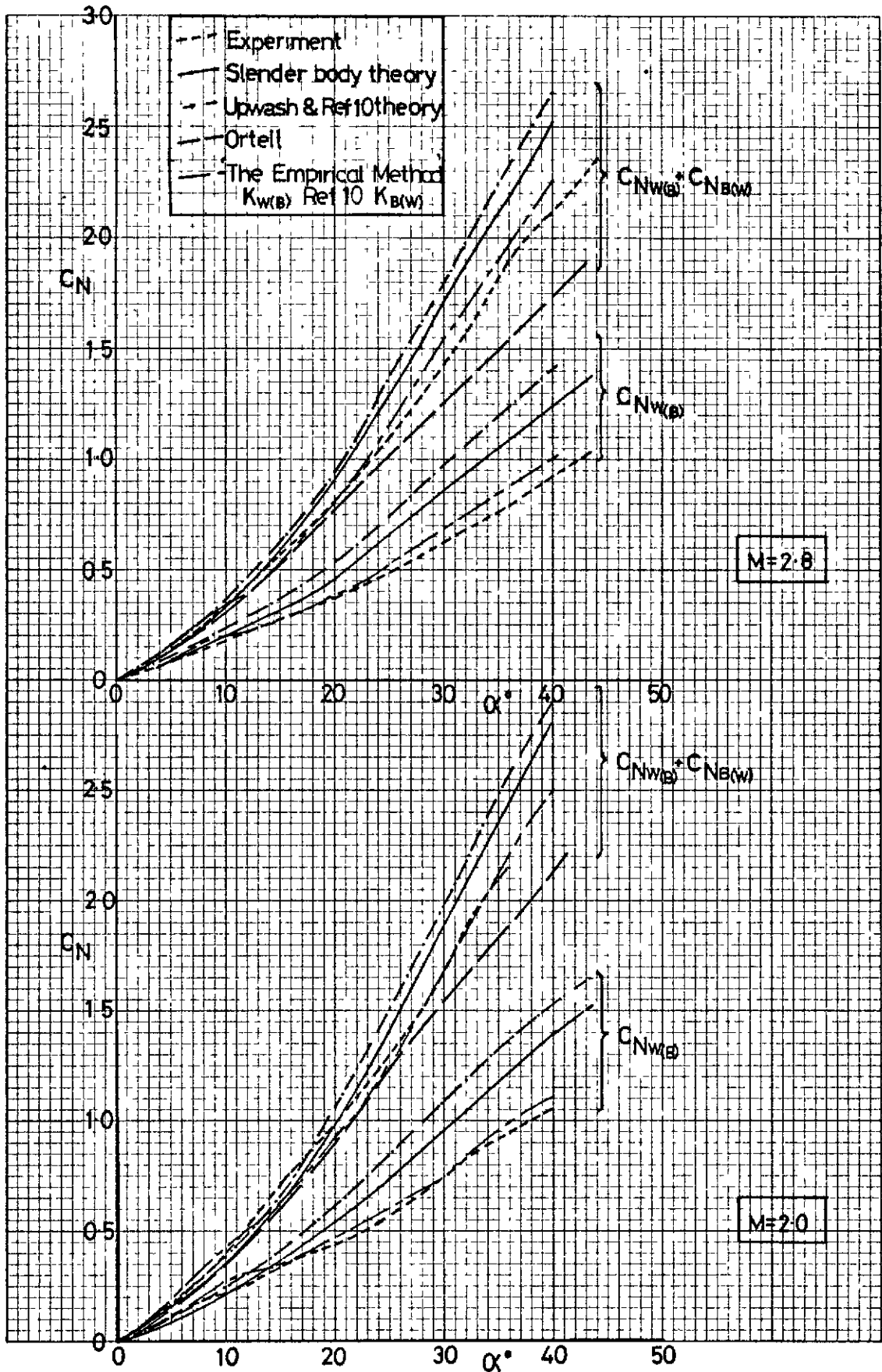


FIG. 25a NORMAL FORCE FOR WING 8 AND PARALLEL BODY COMPARISON OF EXPERIMENT AND THEORY.

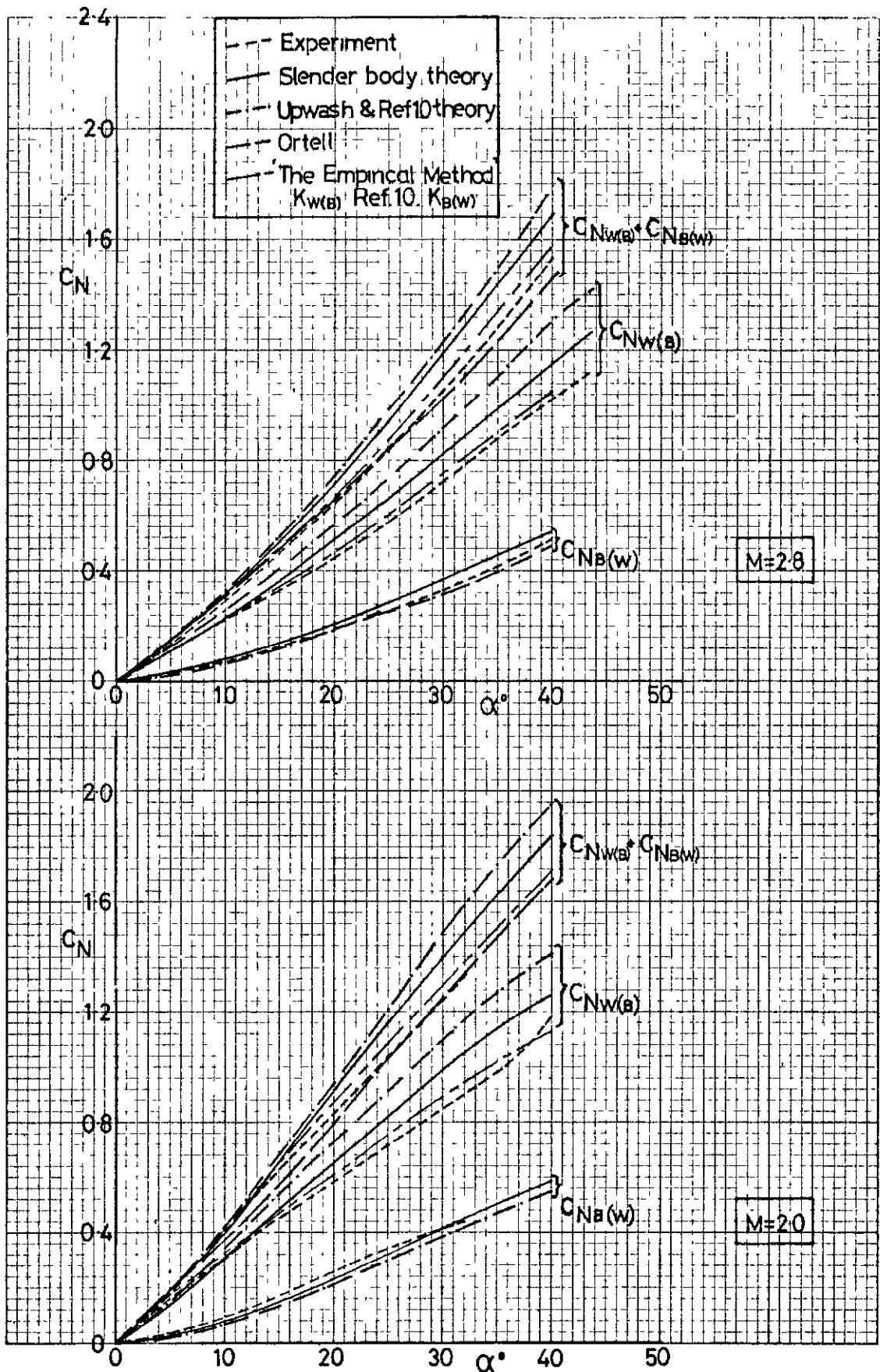


FIG.25b. NORMAL FORCE FOR WING 1 AND PARALLEL BODY COMPARISON OF EXPERIMENT AND THEORY

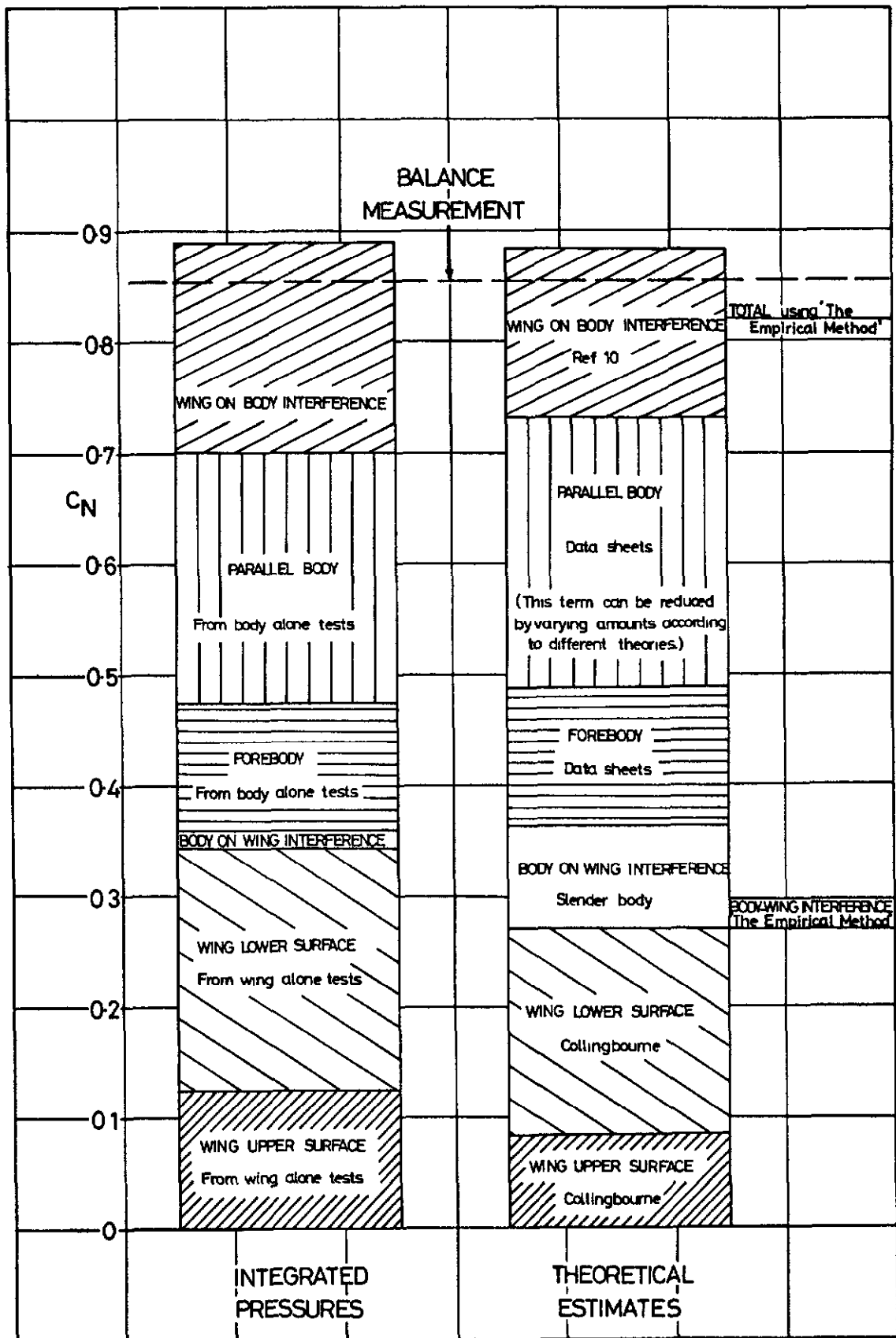


FIG 26. BREAKDOWN OF NORMAL FORCE ON COMPLETE CONFIGURATION WING 8 ON BODY $M=2.8$ $\alpha=20^\circ$

A.R.C. C.P. No.1131

November, 1969

Mrs. K. A. Fellows and E. C. Carter

RESULTS AND ANALYSIS OF PRESSURE MEASUREMENTS ON TWO
ISOLATED SLENDER WINGS AND SLENDER WING-BODY COMBINATIONS
AT SUPERSONIC SPEEDS

As a contribution to the RAE study on guided weapons, this report deals with pressure plotting results on an axisymmetric body and two very slender wings tested in isolation and as wing-body combinations up to very high incidence at supersonic speeds.

It has been possible to isolate the contributions to the overall normal force made by the wing upper surface, wing lower surface, forebody, cylindrical body and the mutual wing-body interference. Each item has been compared/

A.R.C. C.P. No.1131

November, 1969

Mrs. K. A. Fellows and E. C. Carter

RESULTS AND ANALYSIS OF PRESSURE MEASUREMENTS ON TWO
ISOLATED SLENDER WINGS AND SLENDER WING-BODY COMBINATIONS
AT SUPERSONIC SPEEDS

As a contribution to the RAE study on guided weapons, this report deals with pressure plotting results on an axisymmetric body and two very slender wings tested in isolation and as wing-body combinations up to very high incidence at supersonic speeds.

It has been possible to isolate the contributions to the overall normal force made by the wing upper surface, wing lower surface, forebody, cylindrical body and the mutual wing-body interference. Each item has been compared/

A.R.C. C.P. No.1131

November, 1969

Mrs. K. A. Fellows and E. C. Carter

RESULTS AND ANALYSIS OF PRESSURE MEASUREMENTS ON TWO
ISOLATED SLENDER WINGS AND SLENDER WING-BODY COMBINATIONS
AT SUPERSONIC SPEEDS

As a contribution to the RAE study on guided weapons, this report deals with pressure plotting results on an axisymmetric body and two very slender wings tested in isolation and as wing-body combinations up to very high incidence at supersonic speeds.

It has been possible to isolate the contributions to the overall normal force made by the wing upper surface, wing lower surface, forebody, cylindrical body and the mutual wing-body interference. Each item has been compared/

DETACHABLE ABSTRACT CARDS

compared with theoretical and empirical prediction methods currently available. Significant differences between theory and practice were discovered, particularly for the most slender wing, at high pitch angles.

The vortex induced lift on the wing upper surface continues up to very high incidences especially on the most slender wing, with much higher suction than had been predicted. New values of k , the limiting suction level, are proposed and an empirical formula relating the upper surface normal force to Mach number, leading edge sweep angle and pitch angle is suggested for the range of these particular wings.

Body interference on the wing falls off rapidly above about 10° but there is no loss of non-linear lift on the body due to the presence of the wings.

compared with theoretical and empirical prediction methods currently available. Significant differences between theory and practice were discovered, particularly for the most slender wing, at high pitch angles.

The vortex induced lift on the wing upper surface continues up to very high incidences especially on the most slender wing, with much higher suction than had been predicted. New values of k , the limiting suction level, are proposed and an empirical formula relating the upper surface normal force to Mach number, leading edge sweep angle and pitch angle is suggested for the range of these particular wings.

Body interference on the wing falls off rapidly above about 10° but there is no loss of non-linear lift on the body due to the presence of the wings.

compared with theoretical and empirical prediction methods currently available. Significant differences between theory and practice were discovered, particularly for the most slender wing, at high pitch angles.

The vortex induced lift on the wing upper surface continues up to very high incidences especially on the most slender wing, with much higher suction than had been predicted. New values of k , the limiting suction level, are proposed and an empirical formula relating the upper surface normal force to Mach number, leading edge sweep angle and pitch angle is suggested for the range of these particular wings.

Body interference on the wing falls off rapidly above about 10° but there is no loss of non-linear lift on the body due to the presence of the wings.

© *Crown copyright 1970*

Printed and published by
HER MAJESTY'S STATIONERY OFFICE

To be purchased from
49 High Holborn, London WC1V 6HB
13a Castle Street, Edinburgh EH2 3AR
109 St Mary Street, Cardiff CF1 1JW
Brazennose Street, Manchester M60 8AS
50 Fairfax Street, Bristol BS1 3DE
258 Broad Street, Birmingham 1
7 Linenhall Street, Belfast BT2 8AY
or through booksellers

Printed in England